minerals

MDPI

Article

Trace Element Contents in Sphalerite from the Nayongzhi Zn-Pb Deposit, Northwestern Guizhou, China: Insights into Incorporation Mechanisms, Metallogenic Temperature and Ore Genesis

Chen Wei [1,2], Zhilong Huang [1,*], Zaifei Yan [1], Yusi Hu [1,2] and Lin Ye [1]

[1] State Key Laboratory of Ore Deposit Geochemistry, Institute of Geochemistry, Chinese Academy of Sciences, Guiyang 550081, China; weichen@mail.gyig.ac.cn (C.W.); zaifeiyan@163.com (Z.Y.); huyusi@mail.gyig.ac.cn (Y.H.); yelin@vip.gyig.ac.cn (L.Y.)

[2] University of Chinese Academy of Sciences, Beijing 100049, China

* Correspondence: huangzhilong@vip.gyig.ac.cn; Tel.: +86-851-589-5938; Fax: +86-851-589-1664

Received: 3 September 2018; Accepted: 22 October 2018; Published: 26 October 2018

Abstract: The Nayongzhi Zn-Pb deposit, located in the southeastern margin of the Sichuan-Yunnan-Guizhou (S-Y-G) Zn-Pb metallogenic province, China, has been recently discovered in this region and has an estimated resource of 1.52 Mt of metal at average grades of 4.82 wt % Zn and 0.57 wt % Pb. The ore bodies are hosted in the Lower Cambrian Qingxudong Formation dolostone and occur as stratiform, stratoid and steeply dipping veins. The predominant minerals are sphalerite, galena, dolomite, calcite with minor pyrite, and barite. In this paper, the inductively coupled plasma mass spectrometry (ICP-MS) technique has been used to investigate the concentrations of Fe, Cd, Ge, Ga, Cu, Pb, Ag, In, Sn, Sb, Co and Mn in bulk grain sphalerite from the Nayongzhi deposit, in an effort to provide significant insights into the element substitution mechanisms, ore-forming temperature and genesis of the deposit. This study shows that those trace elements (i.e., Cd, In, Sn, Sb, Fe, Mn, Cu, Ga, Ge, Ag, and Co) are present in the form of isomorphism in sphalerite, and strong binary correlation among some elements suggests direct substitution as $Zn^{2+} \leftrightarrow Fe^{2+}$ and coupled substitutions as $Zn^{2+} \leftrightarrow Ga^{3+} + (Cu, Ag)^{+}$ and $Zn^{2+} \leftrightarrow In^{3+} + Sn^{3+} + \square$ (vacancy), despite there being no clear evidence for the presence of Sn^{3+}. Sphalerite from the Nayongzhi deposit is enriched in Cd, Ge and Ga and depleted in Fe, Mn, In and Co, which is similar to that of the Mississippi Valley-type (MVT) deposit and significantly different from that of the Volcanogenic Massive Sulfide (VMS) deposit, Sedimentary-exhalative (Sedex) deposit, skarn, and epithermal hydrothermal deposit. Moreover, the ore-forming temperature is relatively low, ranging from 100.5 to 164.4 °C, as calculated by the GGIMFis geothermometer. Geological characteristics, mineralogy and trace element contents of sphalerite suggest that the Nayongzhi deposit is a MVT deposit. In addition, according to the geological characteristics, Ag content in sphalerite, and Pb isotope evidence, the Nayongzhi deposit is distinct from the deposits associated with the Indosinian Orogeny in S-Y-G Zn-Pb metallogenic province (e.g., Huize, Daliangzi, Tianbaoshan and Tianqiao deposits), thus, suggesting that multi-stage Zn-Pb mineralization may have occurred in this region.

Keywords: Nayongzhi Zn-Pb deposit; trace elements; ore-forming temperature; Mississippi Valley-type (MVT) deposit; Sichuan-Yunnan-Guizhou (S-Y-G) Zn-Pb metallogenic province

1. Introduction

Sphalerite (ZnS), one of the most common sulfide minerals, is the major ore of zinc, and approximately 95% of all primary zinc worldwide is extracted from sphalerite ores. Previous

studies have shown that the crystal structure of sphalerite could incorporate a broad variety of elements, with the most significant being Fe, Cd, Ga, Ge and In [1–8], along with the presence of some other elements (e.g., Hg, Ag and Cu) [4–7,9–11]. Several studies have noted that substitution of Zn^{2+} by bivalent similar-sized cations (e.g., Pb^{2+}, Cd^{2+} and Co^{2+}) or by coupled substitution mechanisms, which can be extended to tri- and tetravalent elements (e.g., Sb^{3+}, In^{3+} and Ge^{4+}). Moreover, the trace element contents of sphalerite were identified as being related to the temperature of ore formation [7,12–14]. Möller [14] proposed that the Ga/Ge ratio in sphalerite could be used as a geothermometer. However, his treatment assumed that the Ga/Ge ratio in sphalerite and the coexisting hydrothermal fluid should be identical, which given a strong dependence of partition coefficient on various physicochemical parameters, including temperature, seems impractical. Recently, Frenzel et al. [7] offered a new sphalerite geothermometer (GGIMFis), which could be applied to calculate the ore-forming temperature of various deposit types, based on the assumption that Fe, Mn, Ga, Ge, and In are incorporated in the crystal lattice of sphalerite. This geothermometer firstly was used to calculate the ore-forming temperature of the Cristal nonsulfide Zn prospect, Bongará district, northern Peru by Mondillo et al. [8]. Furthermore, it has been recognized relatively recently that the trace element endowment of sphalerite can, to a large extent, be correlated with genetic type [4–6,15,16]. Zhang [16] first attempt to use the trace element contents (e.g., In, Ga, Fe, Cd, Mn) of sphalerite to discriminate the genetic type of Zn-Pb deposit. Subsequently, Cook et al. [4] and Ye et al. [5] confirm that sphalerites from different ore genetic types have significant different trace element contents, which can be used as discriminators among genetic types of ores. However, although a great number of researchers have accessed the trace element contents in sphalerite to understand the ore-forming process and genetic type of ore deposit, the existing form of some elements (e.g., In, Sn, Ga, Ag and Cu) commonly found in sphalerite still remain less well constrained. It is not entirely clear whether they enter the sphalerite structure at all or are almost present as an inclusion of independent mineral, which restricts the application of the geothermometer and discrimination of genetic type.

The Nayongzhi deposit, located in the southeastern margin of the Sichuan-Yunnan-Guizhou (S-Y-G) Zn-Pb metallogenic province, China (Figure 1a), is the largest Zn-Pb deposit in northwestern Guizhou Province. This deposit, exploited by the most recent mining operation, has an estimated resource of 1.52 Mt of metal at average grades of 4.82 wt % Zn and 0.57 wt % Pb [17,18]. The salient aspects of the geological characteristics of the deposit, including ore-controlling factors, ore-forming material and fluid source, and mining projects of the Nayongzhi deposit, have been discussed in a number of papers [17–25]. Some authors consider that the metals were mainly derived from the basement rocks based on the Pb isotopic results of sulfides [17,18]. Meanwhile, the S isotopic compositions of sulfides reflect the enrichment of ^{34}S in hydrothermal fluid ($\delta^{34}S_{fluid} > +11.8‰$), and such S isotopic signatures show that thermochemical sulfate reduction (TSR) is the principal mechanism for the formation of S^{2-} [17,18]. However, the genesis of this deposit is still debated. Several remarkable studies have proposed very different genetic models, including Sedimentary-exhalative (Sedex) [23], sedimentation-hydrothermal reformation [24] and Mississippi Valley-type (MVT) lead-zinc deposit models [25].

In this paper, an integrated geological and geochemical study was carried out on the Nayongzhi deposit. Electron microprobe analysis (EMPA) and inductively coupled plasma mass spectrometry (ICP-MS) were used to obtain the contents of main and trace elements in sphalerite from the Nayongzhi deposit. We aim to constrain the trace elements (e.g., Fe, Ga, In, Sn, Ag and Cu) substitution mechanisms, and attempt to calculate the ore-forming temperature of the Nayongzhi deposit using the GGIMFis geothermometer. Finally, by combining with the trace element characteristics of sphalerite, mineralogy and the geological features of the deposit, we can discriminate the ore genetic type, giving new insights into the Zn-Pb mineralization in the S-Y-G Zn-Pb metallogenic province.

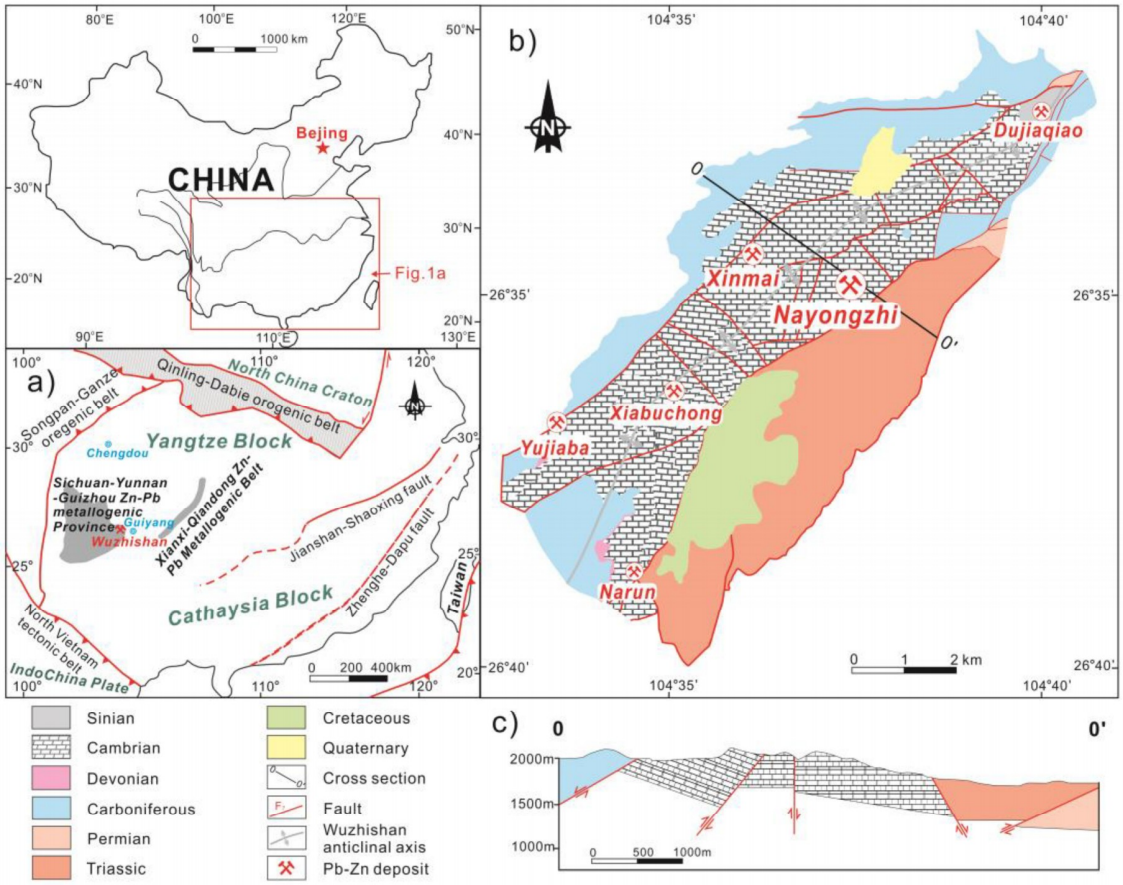

Figure 1. (**a**) Simplified geological map of the South China Craton and adjacent regions showing the framework and the distribution of MVT Zn-Pb deposits in the Yangtze Block (Ye et al. [5] and Hu et al.; (**b**) The geological map of the Wuzhishan anticline showing the location of zinc-lead deposits; (**c**) Geologic cross section 0-0′ showing the Wuzhishan anticline.

2. Regional Geology

The South China Craton is composed of the Yangtze Block in the northwest and the Cathaysia Block in the southeast. To the north, the early Mesozoic Qinling-Dabie Orogenic Belts lie between the Yangtze Block and the North China Craton. To the west, the Yangtze Block is bounded by the Tibetan tectonic domain (Figure 1a). The Yangtze Block is dominated by a Mesoproterozoic to early Neoproterozoic basement overlain by the middle Neoproterozoic weakly metamorphosed strata, the late Neoproterozoic unmetamorphosed Sinian, and Phanerozoic cover [18,26].

The S-Y-G Zn-Pb metallogenic province, located in the southwestern margin of the Yangtze Block, covers over 170,000 km^2 and consists of NE Yunnan, SW Sichuan, and NW Guizhou [27,28]. This area is confined by the NW-SE trending Weining-Shuicheng, the N-S trending Anninghe and the NW-SE trending Mile-Shizong, and the three regional fault belts extend deep into basement rocks. In addition, there are also numerous secondary NE-SW and NW-SE trending faults and thrust-fold belts [18].

In the S-Y-G region, the basement is composed of Mesoproterozoic to the Neoproterozoic Kunyang Group and their equivalents [29,30], which mainly consist of sandstone, siltstone, slate, shale, dolostone, and minor tuffaceous volcanic rocks with a total thickness of about 20 km, and experienced greenschist facies meta-morphism. During the Sinian to Late Permian, the western Yangtze Block was a passive continental margin, leading to the deposition of thick shallow marine sedimentary sequences [31], the unconformity of which covers the basement and are dominated by carbonates and clastic sediments [32]. They are overlain by the Permian Emeishan flood basalt, a product of mantle plume, which formed at ca. 260 Ma [33] and covered more than 250,000 km^2 [34,35]. During the late Triassic to Cenozoic, the western Yangtze Block was affected by the Indosinian Orogeny and the India-Asia collision, resulting in the deposition of continental facies, including terrigenous sandstones, conglomerates, and freshwater marls [36].

More than 400 Zn-Pb deposits are distributed in the S-Y-G Zn-Pb metallogenic province which are hosted in Sinain to Lower Permian carbonate or, rarely in siliceous carbonate rocks that spatially coexist with the Late Permian Emeishan flood basalts. These deposits are characterized by irregular ore bodies with simple mineral assemblages, weak wall rock alteration, controlled by thrust-fold tectonic fractures [37,38] and a high Pb + Zn ore grade [27,39] usually associated with Ag, Ge, Cd, Ga and In [15,28].

3. Geology of the Nayongzhi Deposit

The Nayongzhi deposit (26°25′ N, 105°38′ E) is located in the southeast margin of S-Y-G region, 40 km north-northwest of Puding city. The ore deposit is situated on the NE-trending asymmetric Wuzhishan overturned anticline (Figure 1b) that trends 315° with an axial plane dipping to the SE (Figure 1c); this anticline is 16 km in length and 4 km in width, where are distributed several lead-zinc deposits (e.g., Dujiaqiao, Nayongzhi, Xinmai, Xiabuchong, Yujiaba and Narun ore deposits; Figure 1b).

3.1. Strata and Structures

The dip angle of the SE wing ranges from 15° to 23°. Major faults in the area include the regional NE-trending Jichangpo fault, a subsidiary fault of the NW-trending fault, and a minor secondary NE-trending fault. The Jichangpo fault, which is characterized by a high dip angle (40°–65°) and normal fault character, is over 6 km length and 1–5 m in width [23,25].

The exposed strata in the Nayongzhi mining district range from Sinian to Carboniferous (Figure 2). The Upper Sinian Dengying Formation is a light gray thick-bedded coarse-grain dolostone overlain by Lower Cambrian, which was divided into four parts from bottom to top: (1) the Lower Cambrian Niutitang Formation, predominantly composed of black charcoal shale, grayish green silty claystone and black coarse-grain charcoal limestone, 30–50 m in thickness; (2) the Lower Cambrian Mingxinsi Formation, composed of yellow silty claystone, quartz sandstone and gray medium-bedded oolitic limestone, 150–170 m in thickness; (3) the Lower Cambrian Jinding Formation, consisting of argillaceous siltstone, quartz sandstone and limestone, over 150 m in thickness; (4) the Lower Cambrian Qingxudong Formation, which is the principal ore hosting sequence at the Nayongzhi deposit (Figure 3), and is predominantly composed of grayish white fine-grain dolostone, over 373.9 m in thickness. Notable unconformity is present between the Lower Cambrian Qingxudong Formation and Lower Carboniferous Xiangbai Formation. The Lower Carboniferous Xiangbai Formation is composed of gray mudstone, and argillaceous siltstone, and quartz sandstone, 1–10 m in thickness; the Lower Carboniferous Dapu Formation, overlain on the Lower Carboniferous Xiangbai Formation, is composed of light gray-gray white middle-thick coarse-grain dolostone interlayer dolomitic limestone, yellow shale and argillaceous siltstone, 30–100 m in thickness.

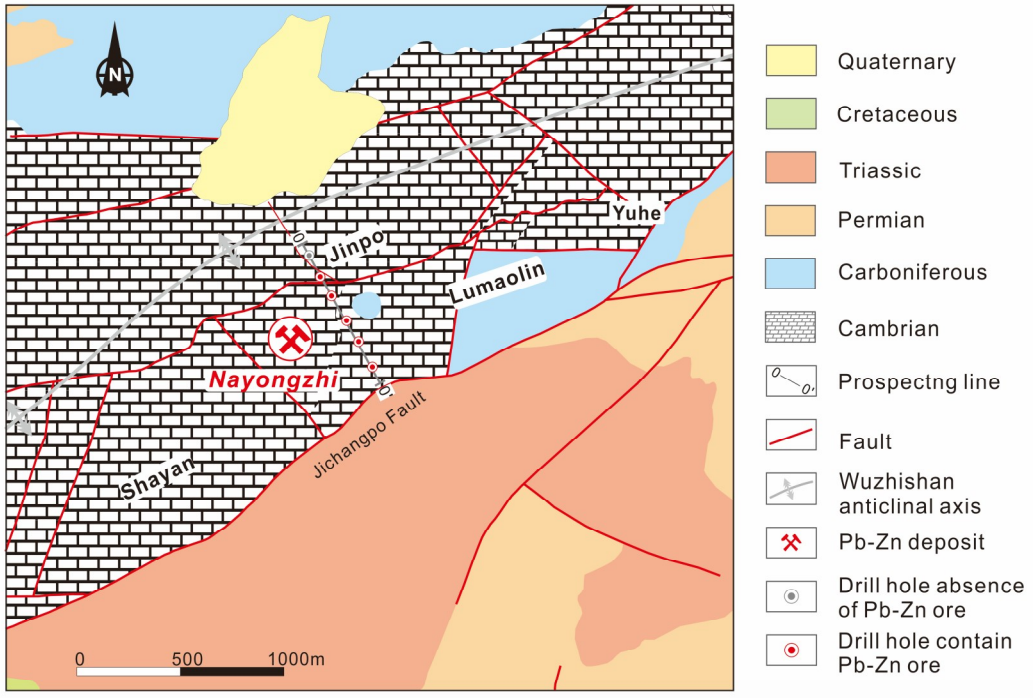

Figure 2. Geological sketch map of the Nayongzhi district (modified from Jin et al. [17]), showing the distribution of ore blocks, strata, faults.

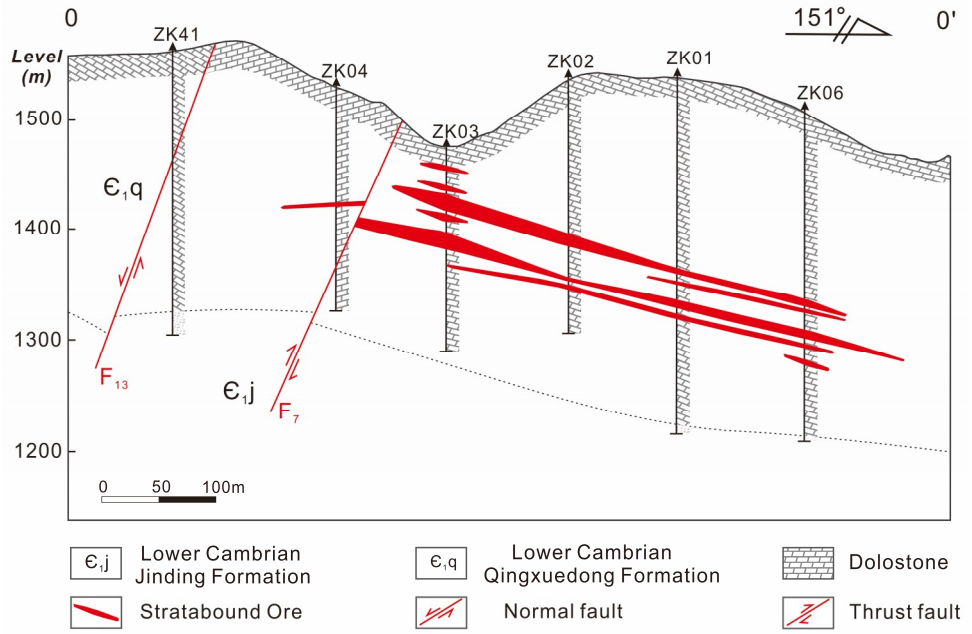

Figure 3. Geologic cross section 0-0′ through the Nayongzhi deposit, revealing the distribution of ore bodies, faults and strata (modified from Jin et al. [17]).

3.2. Ore Bodies, Ore Types and Mineralogy

The Nayongzhi orefield mainly includes four ore blocks, respectively, for Shaya, Jinpo, Lumaolin, and Yuhe ore blocks (Figure 2). The Shaya ore block is situated in the southwest part of the mining area, where the ore bodies are typically 40–980 m in length and 0.75–13.5 m in thickness; the Pb + Zn resources of these bodies exceed 0.53 Mt, with the average grade of Zn 5.62 wt % and Pb 0.99 wt %. The Jinpo ore block is in the central part of the mining area, where the ore bodies are 50–1266 m in length and 1.0–21.3 m in thickness; the Pb + Zn resources of these bodies exceed 0.44 Mt with

the average grade of Zn 5.60 wt % and Pb 0.64 wt %. The Lumaolin ore block is in the northeast part of the mining area, where the ore bodies are 50–1034 m in length and 0.35–11.5 m in thickness; the Pb + Zn resources of these bodies exceed 0.38 Mt, with the average grade of Zn 4.0 wt % and Pb 0.6 wt %. The ore bodies occur as lenticular, stratiform and parallel to the surrounding strata in Shayan, Jinpo and Lumaolin ore block. (Figure 3). In addition, the farthest northeast of the mining area is the Yuhe ore block, where the ore bodies are hosted within the fault fracture zone and extensive deepening long than 200 m. The Pb + Zn resources of this ore block are approximately 0.17 Mt, with the average grade of Zn 13.8 wt % and Pb 3.1 wt %.

Mineralization occurs in massive ores (Figure 4a,g), breccias (Figure 4b–e), disseminated ores (Figure 4f) and veins (Figure 4h,i) in this deposit. Both sulfide and supergene ore are developed in the Nayongzhi deposit. Primary sulfide minerals are sphalerite, and galena and with minor pyrite in the Nayongzhi deposit (Figure 4a–i). Supergene ore is composed of smithsonite, goethite and cerussite [17]. The common gangue minerals are dolomite, calcite, with minor barite.

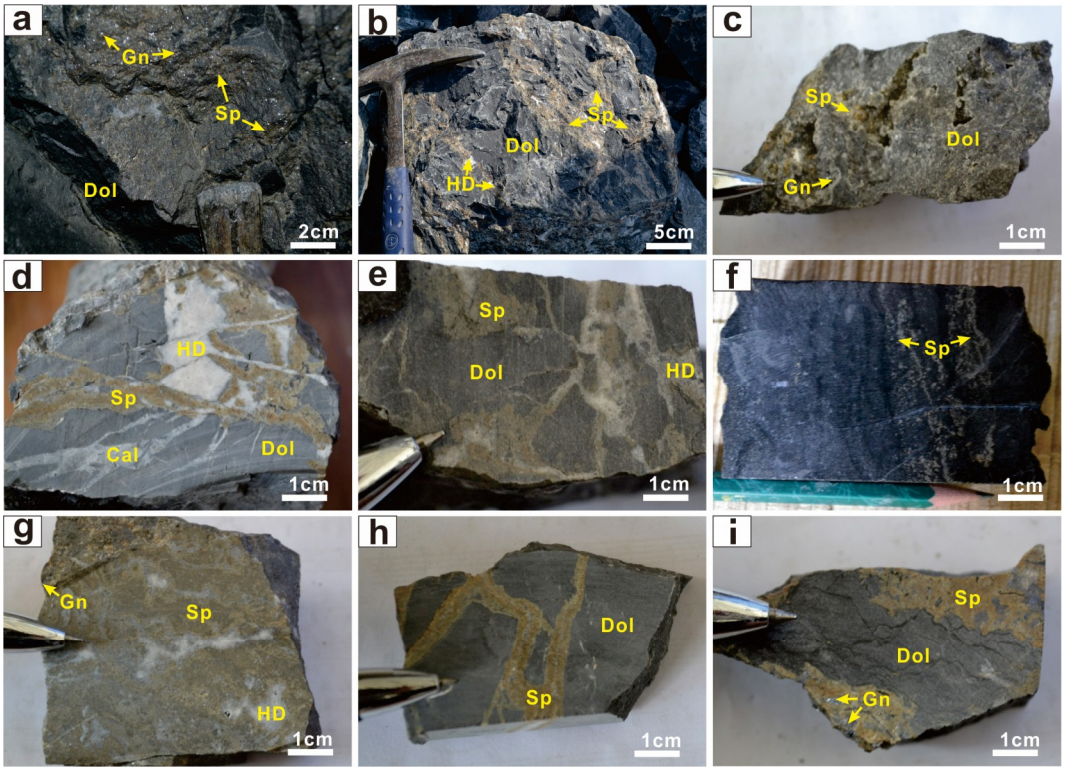

Figure 4. Mineral assemblages and textures of the samples from the Nayongzhi deposit. (**a**) Massive sphalerite and galena assemblage. (**b**) Vein-like Sphalerite and hydrothermal dolomite cemented the fragments of dolostone. (**c**) Fine-grain sphalerite and galena fill the vugs of dolostone. (**d**) Sphalerite and hydrothermal dolomite fill the fractures of the dolostone. (**e**) Stockwork of sphalerite distributed in the fragments of host rock. (**f**) Disseminated sphalerite hosted in the dolostone. (**g**) Massive sulfides including sphalerite and galena. (**h**) Vein sphalerite filling the dolostone. (**i**) Sphalerite-galena assemblage. Abbreviations: Sp Sphalerite; Gn galena; Dol dolostone; HD hydrothermal dolomite; Cal calcite.

The principal ore textures are euhedral-subhedral granular, subhedral-anhedral granular, fragmented texture, and replacement texture. Granular texture is the most common. Sphalerite is characteristically fine-grained, euhedral-subhedral-anhedral granular, which is wrapped by calcite (Figure 5a), hydrothermal dolomite (Figure 5b,g) and pyrite (Figure 5f), or encloses pyrite (Figure 5e). Most sphalerite are light yellow in color, but brownish and brownish red colors are occasionally observed (Figure 5a,b). Galena is euhedral-subhedral granular and veinlets; the individual grain

is 0.1–10 mm diameter and has cubic cleavage (Figure 5c,d,h,i), which is enclosed by hydrothermal dolomite (Figure 5c,d), pyrite (Figure 5d,h) or sphalerite (Figure 5i). Pyrite is fine-grained (0.1–1 mm), and commonly occurs as dissemination or bands in the wall rock adjacent to ores (Figure 5d), or encloses galena (Figure 5d,h); diagenetic pyrite is fine-grained and occurs as dissemination in the wall rock (Figure 5c). Fragmented sphalerite is enclosed by pyrite or hydrothermal dolomite (Figure 5e). Replacement texture is identified, in which sphalerite is replaced by pyrite (Figure 5f) or replaces galena (Figure 5i).

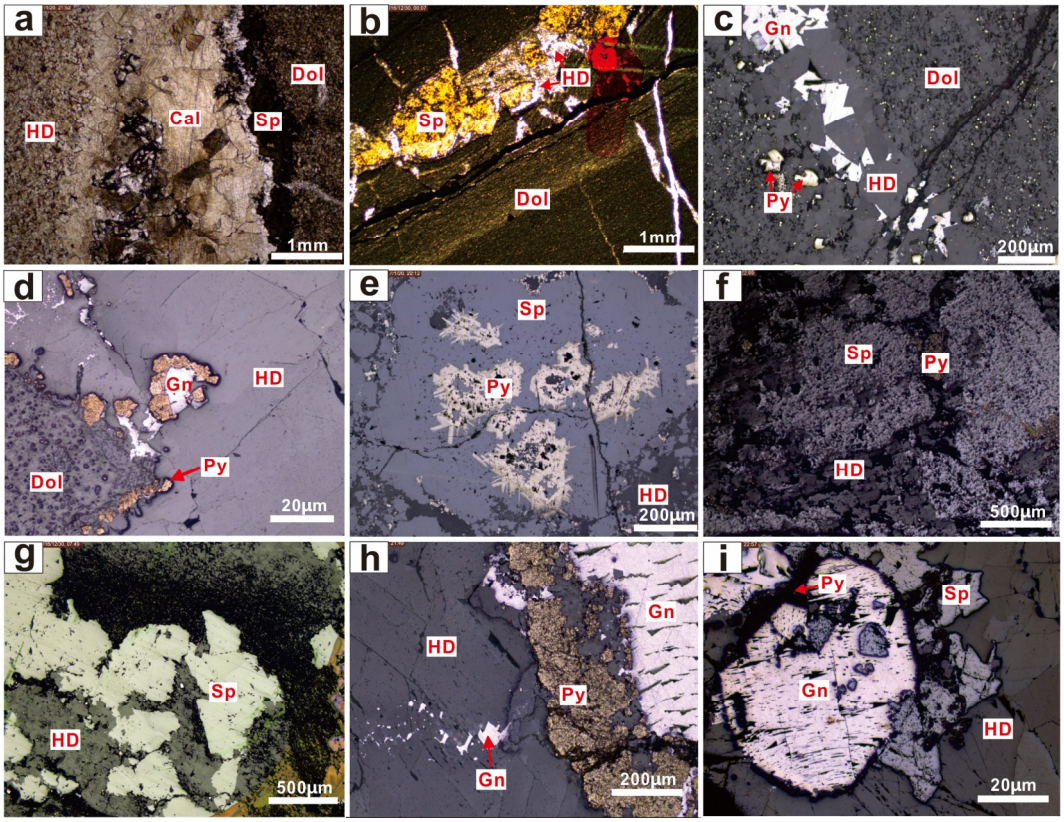

Figure 5. Microphotographs of representative samples from the Nayongzhi deposit. (**a**) Sphalerite and calcite intergrowth with hydrothermal dolomite. (**b**) Euhedral sphalerite and hydrothermal dolomite fill the fractures of dolostone. (**c**) Galena and pyrite fill the fractures of dolostone. (**d**) Galena wrapped by pyrite and hydrothermal dolomite. (**e**) Sphalerite intergrowth with pyrite. (**f**) Pyrite fill the edge of euhedral sphalerite granule (**g**) Euhedral sphalerite is around by hydrothermal dolomite. (**h**) Galena intergrowth with pyrite. (**i**) Galena replaced by sphalerite. Photomicrographs (a,b) were taken under transmitted plane-polarized light, and (c–i) were taken under reflected plane-polarized light. Abbreviations: Sp sphalerite; Gn galena; Py pyrite; Dol dolostone; HD hydrothermal dolomite; Cal calcite.

3.3. Mineral Paragenesis

Based on the field and microscopic observations of crosscutting relationships of veins and paragenetic relationships of various hydrothermal minerals, the mineralization process has been classified into three stages (Figure 6), generally beginning from sedimentary diagenesis through hydrothermal mineralization followed by supergene oxidization, wherein the hydrothermal process can be divided into early-stage and late-stage according to distinct mineral assemblages. The early-stage mineralization is mainly massive ores and brecciated ores (Figure 4a,b,d,g,i), which consist of euhedral to subhedral coarse-grained sulfide minerals aggregates (sphalerite, galena and pyrite; Figure 5a,b,e–g,i), and veins or disseminated ores (Figure 4c,e,f,h) that is composed of subhedral to anhedral fine-grained aggregates (dominated by galena; Figure 5c). In the late-stage

mineralization, gangue mineral hydrothermal dolomite and calcite occur as fragment or fine-veined aggregate cement that fill the fractures and voids of sulfide aggregation or wall rocks (Figure 4a–e,g).

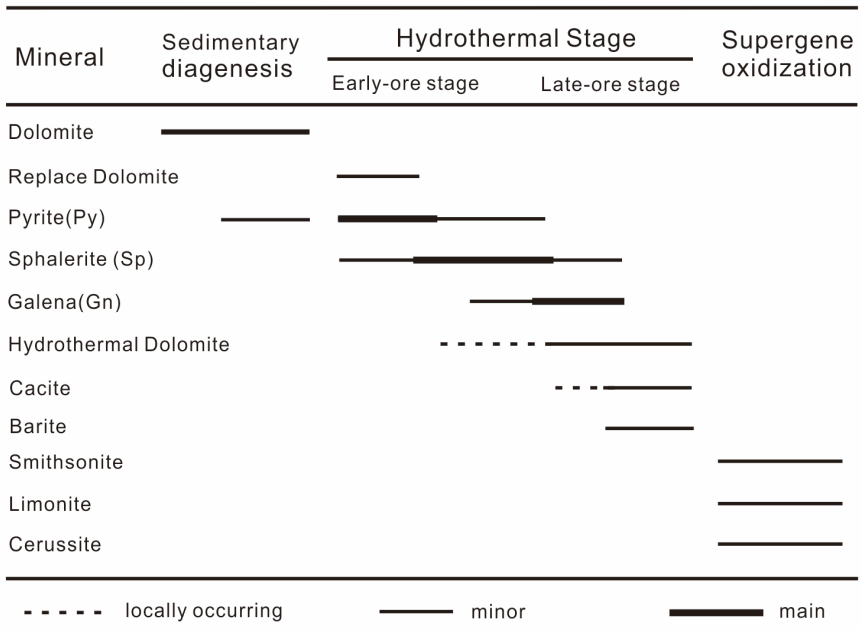

Figure 6. Mineral paragenesis in the Nayongzhi deposit.

4. Sampling and Analytical Methods

The ore-bearing samples were collected from the mining adit at 1390 m and 1270 m and at the ore pile. Thirteen sphalerite samples were crushed to a size of 40–80 mesh, and were handpicked under a binocular microscope with a purity better than 99% for trace element analysis.

4.1. Electron Microprobe Analysis (EMPA)

Preliminary analyses were carried out using an electron microprobe analysis (EPMA) at the State Key Laboratory of Ore Deposit Geochemistry, Chinese Academy of Science (SKLODG), using a 1600 EMPA from the Shimadzu Corporation, Japan. All of the EPMA undertaken during this study was carried out on clear surface areas of representative ore mineral grains. This analysis was performed at an accelerating voltage of 15 kV, with a beam current of 20 nA and a 5 μm diameter electron beam. The limit of detection (LOD) was better than 0.05%.

4.2. Inductively Coupled Plasma Mass Spectrometry (ICP-MS)

The analysis of trace elements in sphalerite were carried out with an ICP-MS (Finnigan MAT, Bremen, Germany) at the National Geological Analytical and Testing Center, Chinese Academy of Geological Sciences, Beijing, using the method of Qi et al. [40]. For sample preparation about 50 mg of powdered sample was dissolved by 1 mL of HF and 1 mL of HNO_3 in a PTFE bomb; then the sealed bombs were heated to 190 °C for about 36 h in an electric oven. After cooling, the bombs were placed on a hot plate to evaporate to dryness. A quantity of 2 mL of HNO_3 and 4 mL of ultrapure water were added, and then 500 ng of Rh was added as an internal standard. The bomb was again sealed and heated to 140 °C for about 5 h in an electric oven to dissolve the residue. After cooling, the final dilute factor was about 3000 for ICP-MS measurements. GSR-5 (Shale, Qi et al. [40]) was used as the external standard, with an analytic precision of greater than 5%. Minimum LOD was usually 100 ppm for Zn and Fe, 1 ppm for the trace elements Cd, Cu, Pb, Mn and Sn, and 0.1 ppm for the trace elements Ga, Ge, Co and Ag. In addition, LOD of In was better than 0.01 ppm analyzed by ICP-MS.

4.3. Principal Components Analysis of Trace Element Datasets

Principal component analysis (PCA), one of most useful multivariate statistical analyses, uses an orthogonal transformation to convert a set of observations of possibly correlated variables into a set of values of linearly uncorrelated variables. It is a powerful variable-reduction technique designed to project data in two-dimensions with minimal data loss. PCA is directly calculated as the eigenvectors of the correlation matrix and are ordered by decreasing eigenvalues. Notably, PCA is the simplest of the true eigenvector-based multivariate analyses. Its operation often can be recognized as revealing the internal structure of the data in a way that best explains the variance in the data. More detailed descriptions of the PCA method can be found in multivariate statistics textbooks [41,42].

PCA is widely used in the field of geochemical exploration on large-scale datasets [43], which helps to better understand the underlying ore mineralization and its organization. Consequently, PCA has also found application in isotope geochemistry [44,45] and sulfide geochemistry [46]. Therefore, we emphasize the use of multivariate statistics to better interpret the trace element data in mineral geochemistry and understand their relationship. Consequently, PCA will be applied to the trace element datasets in our study. All computations were performed using Statistical Product and Service Solutions (SPSS) 21.0 software.

5. Results

5.1. Trace Element Contents

Electron microprobe analysis for some trace elements are listed in Table 1 and Appendix A. The results of EMPA show that the Nayongzhi sphalerite are composed of 64.59 ± 1.01 wt % Zn, which is similar to the content (65.37 ± 0.41 wt %) measured by ICP-MS, and 32.90 ± 0.84 wt % S. Fe were consistently detected with mean concentrations of 1.30 ± 0.98 wt %. Moreover, Cd was detected in 17 spots with contents up to 0.36 wt %; Ge was detected in only 2 spots, with concentration of 500 and 700 ppm.

Table 1. Electron microprobe analysis (EMPA) main results of sphalerite of the Nayongzhi deposit. Minimum, maximum, mean and the corresponding standard deviation (S.D).

	Zn (wt %)	S (wt %)	Fe (wt %)	Cd (wt %)	Ge (ppm)
n	32	32	32	17	2
max	65.63	33.66	2.28	0.36	700
min	63.61	31.98	0.33	0.11	500
mean	64.59	32.9	1.29	0.2	
S.D	2.02	1.67	1.95	0.25	

n: number of measurements with higher contents than the limit of detection.

The trace elements in sphalerite that were determined with ICP-MS are summarized in Table 2, and histograms of the element contents are shown in Figure 7.

Sphalerite displays significant Fe and Cd contents (n × 10^{-3}–n × 10^{-2}), which show a weak anti-correlation (R^2 = 0.45). Fe displays concentrations of 1.42–1.77 wt %, with a mean of 1.57 wt %, and Cd displays concentrations from 774–1140 ppm, with a mean of 939 ppm. On other hand, Pb contents vary widely, from 576 to 7360 ppm, with an average of 1413 ppm, and most of the sample is lower than 1670 ppm, except for one sphalerite sample (SY-35) that is higher than 7360 ppm, which means that it is likely to contain micro-inclusion (e.g., galena) that resulted in the high lead concentration.

Table 2. Elemental composition of bulk grain sphalerite determined with ICP-MS and the ore-forming temperature of the Nayongzhi deposit calculated by the GGIMFis geothermometer [7].

Sample	Zn	Fe	Cd	Cu	Pb	Ga	Ge	Mn	Sb	Co	Ag	In	Sn	PC1 *	T_{Min} (°C)	T_{Max} (°C)
LML-11	65.51	1.47	856	125	805	40.1	73.4	30	18.4	1.1	1.0	0.15	5	1.14	127.7	164.4
SY-22	65.38	1.57	981	144	1140	56.0	108.0	20	10.4	1.0	1.2	0.20	5	1.33	116.4	155.8
SY-23	65.17	1.70	998	155	1060	57.7	200.0	20	9.9	1.1	0.9	0.18	5	1.45	108.8	150.0
LML-8	65.33	1.58	856	98	600	40.4	336.0	30	16.6	1.0	1.0	0.27	4	1.39	112.6	152.9
LML-2	65.13	1.77	774	116	636	34.7	189.0	20	16.0	0.9	1.1	0.15	4	1.33	116.1	155.5
LML-1	65.31	1.64	868	91	1090	33.9	110.5	20	10.4	1.0	0.9	0.10	3	1.28	119.2	157.9
SY-24	65.54	1.42	1140	159	792	75.9	259.0	20	22.1	1.0	1.1	0.28	7	1.59	100.5	143.6
SY-25	65.31	1.63	1010	162	1670	60.5	183.5	20	11.7	1.1	1.0	0.23	6	1.43	110.0	150.9
SY-26	65.54	1.46	1040	153	1080	66.4	157.0	30	13.2	1.0	1.2	0.14	5	1.43	110.0	150.9
LML-9	65.42	1.51	910	122	637	54.9	115.5	30	24.5	1.0	1.1	0.44	7	1.18	125.2	162.5
SY-35	65.51	1.45	976	186	7360	61.7	210.0	30	7.3	0.9	1.1	0.24	6	1.42	110.5	151.3
LML-7	65.41	1.59	905	140	920	50.3	113.5	30	23.2	1.0	0.9	0.34	7	1.17	126.1	163.1
LML-3	65.31	1.61	886	120	576	49.5	186.5	20	21.5	0.9	1.0	0.38	6	1.34	115.6	155.2
Min	65.13	1.42	774	91	576	33.9	73.4	20	24.5	0.9	0.9	0.10	3	1.45	126.1	164.4
Max	65.54	1.77	1140	186	7360	75.9	336.0	30	7.3	1.1	1.2	0.44	7	1.14	100.5	143.6
Mean	65.37	1.57	939	136	1413	52.5	172.5	25	15.7	1.0	1.0	0.20	5	1.35	115.3	154.9
S.D	0.41	0.35	366	95	6784	42.0	262.6	10	17.2	0.2	0.3	0.34	4	0.31	25.6	20.8

Notes: Zn and Fe in wt % and other elements in ppm in the data table.

The trace elements Ga and Ge are relatively enriched, having a range of concentrations from 33.9 to 75.9 ppm with an average of 52.5 ppm, and from 73.4 to 336.0 ppm with an average of 172.5 ppm, respectively. Cu and Sn concentrations range from 91 to 186 ppm, with an average of 95 ppm, and from 3 to 7 ppm, with an average of 5 ppm, respectively. In addition, In, Sb and Mn contents are relatively lower, displaying narrow ranges, from 0.10 to 0.44 ppm (average of 0.20 ppm), 7.3–24.5 ppm (average of 15.8 ppm), and 20–30 ppm (average of 25 ppm), respectively. Interestingly, both Ag and Co display approximately the same range of concentrations, which are uniformly distributed from 0.9 to 1.2 ppm, and from 0.9 to 1.1 ppm, respectively.

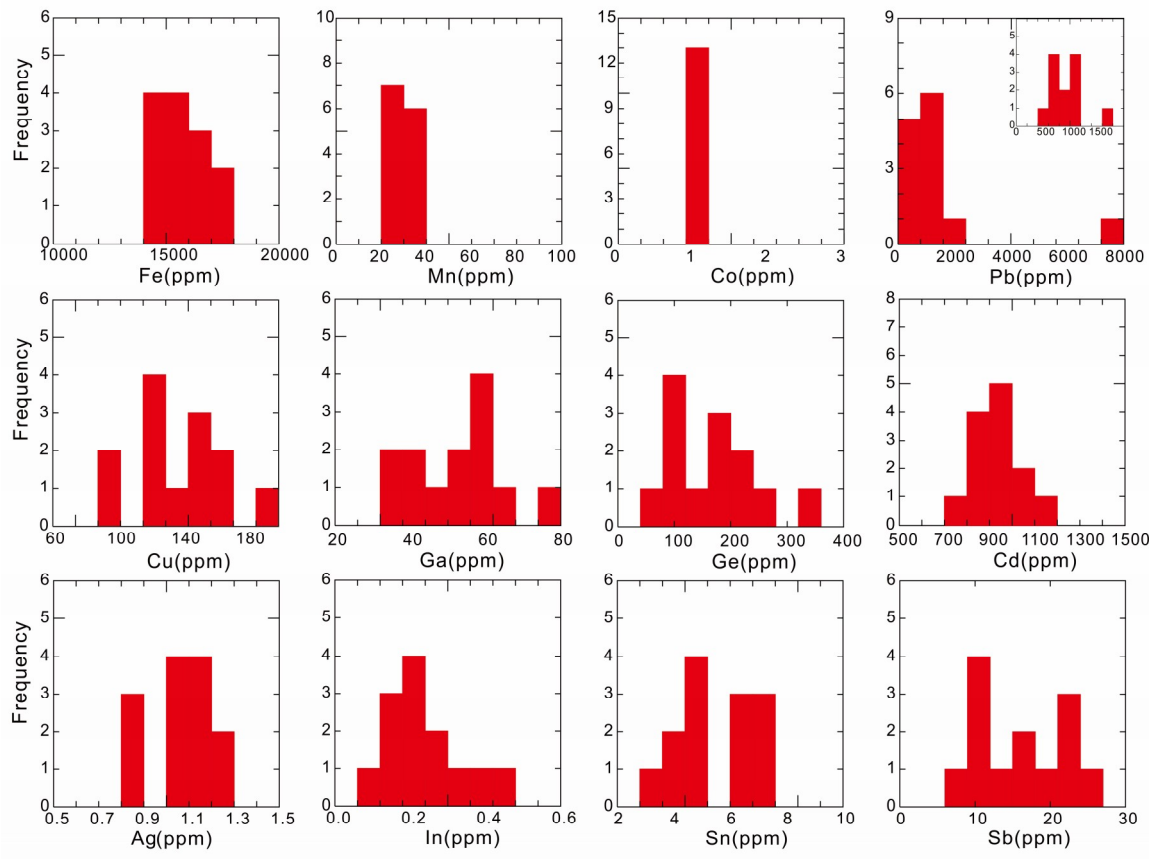

Figure 7. Histogram of trace elements in sphalerite of the Nayongzhi deposit.

5.2. Principal Components Analysis of Trace Elements

The results of the principle components analysis of the ICP-MS dataset are shown in Figure 8, where the element distributions highlight two principal components. Principal Component 1 (PC1) accounts for 52.5% of element content variability (Figure 8a), including Fe, Cu, Ga and Ag (loading PC1; Figure 8b), whereas Principal Component 2 (PC2) accounts for 22.5% of element content variability (Figure 8a), is composed of In and Sn (loading PC2; Figure 8b). Interestingly, PC1 is divided into two sub-groups: (Fe) and (Cu, Ga, and Ag). The element distributions are projected on the PC1 vs. PC2 plane, together accounting for 75.0% of element content variability (Figure 8c).

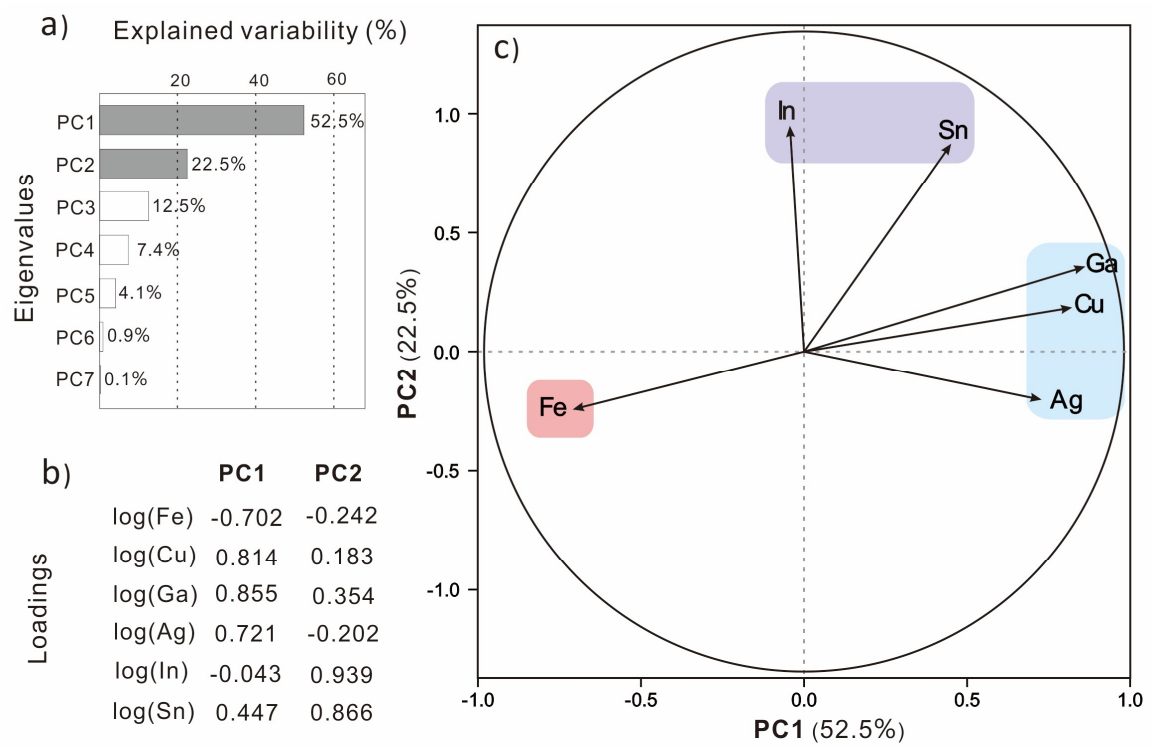

Figure 8. Principal components analysis of the trace element contents (log-transformed) in sphalerite from the Nayongzhi deposit. On the left-hand side edge: eigenvalues (**a**) (i.e., explained variability) and loadings (**b**) (i.e., eigenvector coefficients) of the principal components. Right frame (**c**) elements (i.e., variables) plotted on the PC1 vs. PC2. plane (explaining 75% of the total variability), cluster of elements showing similar behavior are marked as Fe, (In, Sn) and (Ga, Cu, Ag). The angle between two arrows in (**c**) is related to the covariance between the concentrations of the corresponding elements: if the angle is close to 0°, then the elements are positively correlated, if the angle is close to 90°, then they are not correlated, and if it is close to 180°, then they are negatively correlated.

6. Discussion

6.1. Trace Element Substitution Mechanism

The appearance of multi-element correlation groups using PCA (Figure 8b) (i.e., Fe, Cu, Ga and Ag in loading PC1, and In and Sn in loading PC2) may be reasonably associated with trace element incorporation in sphalerite. The small angle among Ga, Cu, and Ag in the PCA confirms the approximate positive correlation, which is consistent with the correlation plot of Ga vs. (Cu + Ag) (Figure 9a). The strong correlation (R^2 = 0.88) between Ga and (Ag + Cu) in sphalerite implies that these three elements are involved in a coupled substitution. In sphalerite, both Cu and Ag likely exist in the +1 state, and Ga likely exists in the +3 state, which have been interpreted [4,10,47,48] as residing in solid solution in sphalerite. The coupled substitution in sphalerite for the case of this deposit may thus be accurately expressed as $2Zn^{2+} \leftrightarrow Ga^{3+} + (Ag, Cu)^{+}$, in agreement with Cook et al. [4].

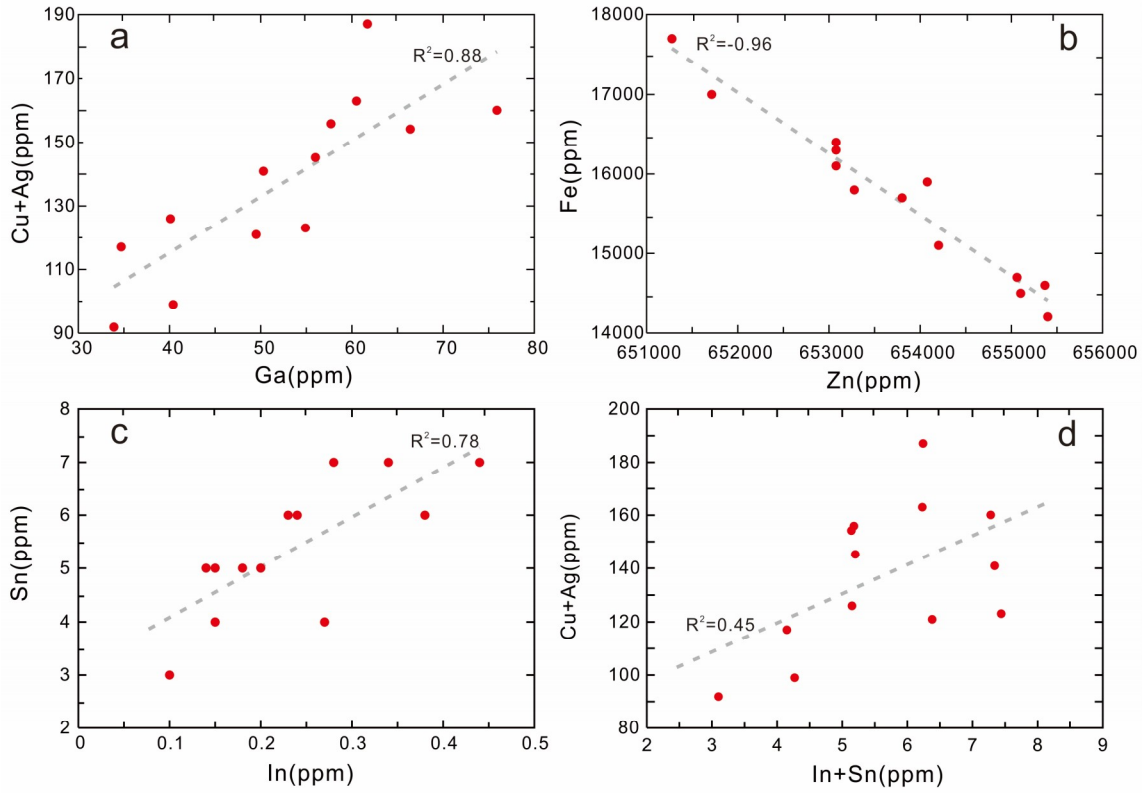

Figure 9. Correlation plots of (**a**) (Cu + Ag) vs. Ga, (**b**) Fe vs. Zn, (**c**) In vs. Sn, (**d**) (In + Sn) vs. (Ag + Cu) in sphalerite from the Nayongzhi deposit. Lines of best fit and R^2 values are given. See the text for further explanation.

Meanwhile, the small angle between In and Sn in the PCA (Figure 8c) is supported by the strong positive correlation that is observed between In and Sn (R^2 = 0.78; Figure 9c). This indicates that sphalerite samples that are rich in Sn are also rich in In. In^{3+} is generally assumed to be present in most minerals [4–6,49]; nevertheless, the main oxidation states of Sn^{2+}, Sn^{3+}, and Sn^{4+} will be somewhat present. Figure 9d shows that there is an unambiguously expressed non-correlation between (In + Sn) and (Cu + Ag), and the involvement of monovalent cations is difficult to verify because Cu and Ag are more concentrated than In and Sn in all samples, which could impossibly involve the following mechanisms: $3Zn^{2+} \leftrightarrow In^{3+} + Sn^{2+} + (Cu, Ag)^{+}$ or $4Zn^{2+} \leftrightarrow In^{3+} + Sn^{4+} + (Cu, Ag)^{+} + \square$ (where $\square$ denotes a vacancy). Consequently, the correlation between In and Sn suggests a potential coupled substitution $3Zn^{2+} \leftrightarrow In^{3+} + Sn^{3+} + \square$, which is consistent with previous study results [13]. The oxidation state of Sn is problematic and requires further work using X-ray absorption near edge structure (XANES)/X-ray photoelectron spectroscopy (XPS) as in Goh et al. [50], Cook et al. [10] and more recently in Belissont et al. [11].

The strong anti-correlation between Zn and Fe (R^2 = −0.96; Figure 9b) in our data support specific studies on trace element incorporation in sphalerite [6,8,51,52], which is suggestive of a direct substitution of divalent cations as $Zn^{2+} \leftrightarrow Fe^{2+}$ (Figure 8c). Moreover, Figure 10 shows that the strong negative correlation is observed among (Cd + In + Sn + Sb + Fe + Mn + Cu + Ga + Ge + Ag + Co) and Zn (R^2 = −0.94), which suggests that those trace elements (Cd, In, Sn, Sb, Fe, Mn, Cu, Ga, Ge, Ag and Co) mainly exist in the form of isomorphism in sphalerite that is thought to be involved in the mechanism of their enrichment in sphalerite [4,5,53,54]. In addition, these elements of sphalerite that generally occur in obscure valences, such as Sb, Mn, and Tl, will need to have their oxidation states accurately determined by appropriate methods (e.g., X-ray absorption spectrum) in the future.

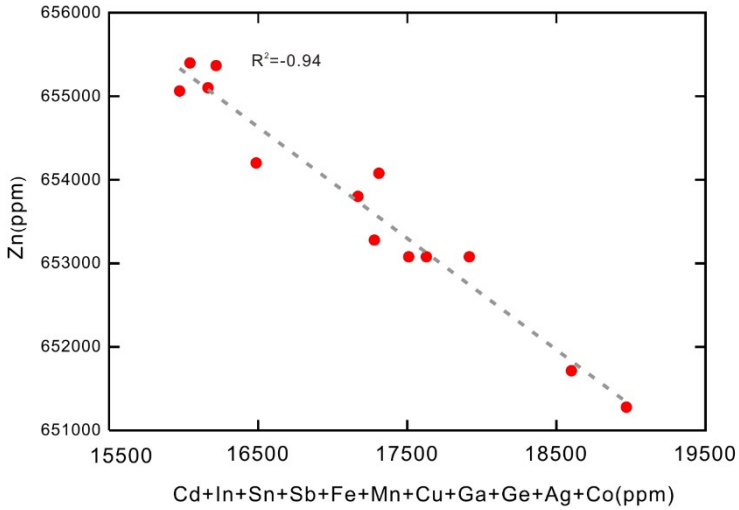

Figure 10. Correlation plots of Zn vs. (Cd + In + Sn + Sb + Fe + Mn + Cu + Ga + Ge + Ag + Co) in sphalerite from the Nayongzhi deposit. Lines of best fit and R^2 values are given. See the text for further explanation.

6.2. Ore-Forming Temperature

Some of the early researchers [12,13] suggested that the trace elements in sphalerite have a close relationship with the ore-forming temperature. They ascribed an association of high Ga and Ge, and low Fe, In and Mn concentrations to "low temperature" deposits, and an association of low Ga and Ge, and high Fe, In and Mn concentrations to "high temperature" deposits. This suggestion was based on the geological criteria and never substantiated by relevant thermometric data or appropriate statistical analyses, whereas Frenzel et al. [7] indicated that the concentrations of Ga, Ge, Fe, Mn and In of sphalerite chemistry are strongly controlled by fluid temperature; the results of the principal components analysis demonstrate that the first principal component of the dataset (PC1) is strongly correlated with the homogenization temperature of the fluid inclusion(R^2 = 0.82, $P < 2 \times 10^{-16}$). It may be expressed as follows: PC 1* = $\mathrm{In}\left(\frac{C_{Ga}^{0.22} \cdot C_{Ge}^{0.22}}{C_{Fe}^{0.37} \cdot C_{Mn}^{0.20} \cdot C_{In}^{0.11}}\right)$ with Ga, Ge, In and Mn concentrations in ppm, and Fe concentration in wt %. The relationship is sufficiently strong that it could be used as a geothermometer (GGIMFis). The empirical relationship between PC1* and temperature (T) is as follows: T(°C) = $-(54.4 \pm 7.3) \times$ PC 1* + (208 ± 10).

As mentioned above, the trace element contents in sphalerite from the Nayongzhi deposit, characterized by rich Cd (774–1140 ppm), Ge (73.4–336.0 ppm), Ga (33.9–75.9 ppm), and low In (0.10–0.44 ppm), Co (0.9–1.1 ppm), Mn (20–30 ppm), and especially Fe (in the range between 14,200 and 17,700 ppm, which is much lower than the high temperature origin of marmatite (Fe concentration exceeds 10 wt %)), is similar to the MVT deposit (e.g., the Niujiaotang deposit in east Guizhou with an ore-forming temperature lower than 150 °C; Ye et al. [55]). Furthermore, the ore-forming temperature of the Nayongzhi deposit is shown in Table 2 and Figure 11; it ranges from 100.5 to 164.4 °C calculated by the trace element geothermometer (GGIMFis) [7], which is close to the homogenization temperature of fluid inclusions in sphalerite from this deposit (102.1–155.2 °C, Wei. [56]). In summary, the Nayongzhi deposit should be considered a low temperature deposit, with ore-forming temperatures between 100.5 and 164.4 °C, in accordance with the metallogenic temperature of a typical MVT deposit (90–150 °C) [57].

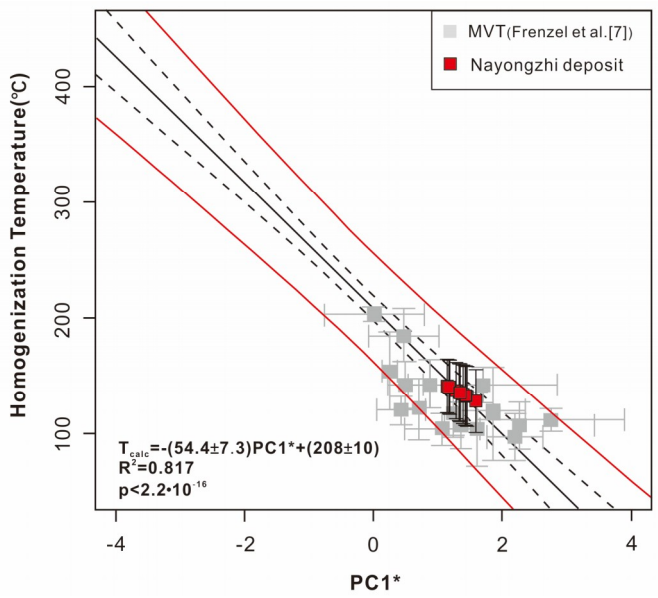

Figure 11. The homogenization temperature of the Nayongzhi deposit showing the GGIMFis geothermometer (modified after Frenzel et al. [7]). Note: the prediction intervals of linear fit are shown as the red lines. 95% confidence intervals are shown as the black dotted lines, while the line of best fit is shown as the black line.

6.3. Genetic Type of Deposit

In discrimination of genetic type of ore deposit, the trace elements in sphalerite show good application prospects [4–6,15,16]. Cook et al. [4] noted that trace element contents in sphalerite from different genetic types of deposit have obvious differences. Subsequently, Ye et al. [5] demonstrated that sphalerite from each genetic type of deposit shows a distinct chemical signature, e.g., the skarn deposits feature is high Co and Mn; their distal character is reflected by low In. The syngenetic massive sulfides deposit is characterized by elevated In, Sn and Ga, whereas the MVT deposits are typically enriched in Ge, Cd, Tl, and As. Consequently, trace elements in sphalerite show promise as a tracer for genetic type of mineral deposits.

Sphalerite from the Nayongzhi deposit is characterized by low In, Co and Mn, which is distinct from the syngenetic massive sulfides and magmatic hydrothermal deposits (In > 50 ppm and Mn > 1000 ppm; Frenzel et al. [7] and Ye et al. [15]), and differs from the distal skarn deposits (Co > 200 ppm and Mn > 1000 ppm; Ye et al. [15]); this sphalerite is the relatively rich Cd, Ge, and Ga that show strong similarities with MVT deposits (Ge > 45 ppm and Cd > 2700 ppm; Frenzel et al. [7] and Ye et al. [15]). The samples from the Nayongzhi deposit, similar to the Niujiaotang Zn-Cd deposit, the notable MVT deposit in China, are located in an MVT deposit area (e.g., Mengxing, Huize and Tianbaoshan deposit, China; Ye et al. [5,15]) in the trace discrimination diagram of Ag-Mn, In/Cd-Mn, In/Ge-Mn, and In + Sn-Mn (Figure 12), and they are distinct from the Volcanogenic Massive Sulfide (VMS) deposits (e.g., Vorta. S. Romaina; Eskay Creek,BC; Sauda, Western Norway; Bergslagen district; Laochang deposit, China; Cook et al. [4] and Ye et al. [5]) and Sedex deposits (e.g., Dabaoshan deposit, China; Ye et al. [5]); in addition, they are even more clearly different from the epithermal deposits (e.g., Neogene epithermal mineralization, East Carpathians; Toyoha Cu-Zn-In deposit, Japan; Cook et al. [4]) and skarn/distal skarn deposits (e.g., Majdanpek, Serbia; Ocna de Fier and Baita Bihor, Romaina; Kamioka, Japan; Konnerudkollen, Norway; Lefevre, Canada; Bainiuchang and Luziyuan deposit, China; Cook et al. [4] and Ye et al. [5]).

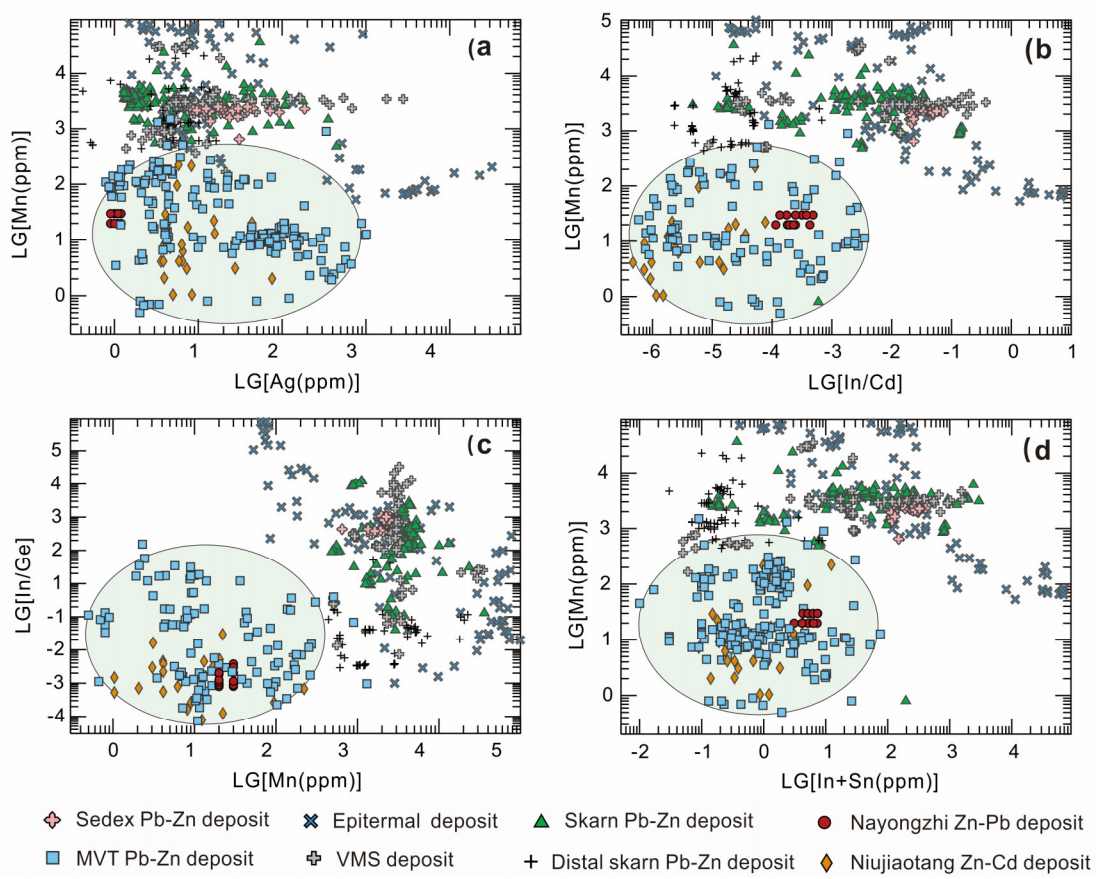

Figure 12. Binary plots of Ag vs. Mn (**a**), In/Cd vs. Mn (**b**), In/Ge vs. Mn (**c**), and In + Sn vs. Mn (**d**) in sphalerite from the Nayongzhi deposit and other Zn-Pb deposits in China, NE Europe, and Japan. Note: plots are based on data from Cook et al. [4] and Ye et al. [5,15].

As noted above, the most important characteristics of the Nayongzhi deposit include: (1) the steeply dipping veined Zn-Pb ore body cutting cross the carbonate rocks was developed, which shows a epigenetic origin; (2) low ore grade and dominated by zinc, with minor Pb; (3) ore bodies in conformity with the country rocks in attitude, occurring as bedded or bed-like formations; (4) simple mineral assemblage, with dominant minerals of sphalerite, galena, dolomite, calcite, and rarely pyrite and barite; (5) coarsely crystalline to fine-grained, massive, brecciated and disseminated sulfides; and (6) alterations consisting mainly of dolomitization, host-rock dissolution and brecciation. Isotopic data indicate the metal displays the upper crust source, most likely derived from the basement rocks, and reduced sulfur in the ore-forming fluid was likely the product of marine sulfate in the ore hosting Cambrian and Sinian strata by thermal-chemical reduction [17,18]. These features of the Nayongzhi deposit are consistent with those of the typical MVT deposit [57–59]. Combined with the evidence of geology, Pb, S isotopes and trace elements in sphalerite, the Nayongzhi deposit should be described as a MVT lead-zinc deposit.

6.4. A New Discovery of a Zn-Pb Mineralization Event in the S-Y-G Metallogenic Province?

Several studies reveal that the collision of the Indochina Block with the South China Block (Indosinian Orogeny) triggered regional migration of the basinal brines that leached ore-forming elements from basement rock to form the S-Y-G Zn-Pb metallogenic province [60,61]. The major features of those deposits (Table 3) are the following: (1) they occur in foreland thrust belts; (2) the majority of the ore bodies are vein-type, controlled by faults cutting the Upper Sinian, Carboniferous and Permian dolostone and limestone sequences; (3) high Pb + Zn ore grades (10–30 wt %), ore grades of a few deposits (e.g., Huize; Han et al. [28]) exceeded 50 wt %; (4) temperatures of ore deposition are typically

150 °C to 270 °C; and (5) ore-fluids were basinal brines with 6.0 to 20 wt % NaCl eqv. In contrast, there are noticeable differences between the Nayongzhi deposit and other Zn-Pb deposits particularly for the geological setting, morphology of ore bodies, the grade of ore, ore-forming temperature, and ore-controlling structure along the S-Y-G Zn-Pb metallogenic province.

Moreover, the Ag contents of sphalerite from Nayongzhi deposit are very low, ranging from 0.9 to 1.2 ppm, whereas the other Zn-Pb deposits (e.g., Huize, Daliangzi, Tianbaoshan and Tianqiao deposit) in S-Y-G district are relatively enriched in Ag, which is one or two order of magnitude higher than that of the Nayongzhi deposit (Figure 13). Meanwhile, the Pb isotope ratio of sulfides (sphalerite, pyrite and galena) in the Nayongzhi deposit are 17.828 to 17.924 for $^{206}Pb/^{204}Pb$, 15.640 to 15.707 for $^{207}Pb/^{204}Pb$, and 37.922 to 38.176 for $^{207}Pb/^{204}Pb$ [17,18,24,62], which are significantly lower than that ($^{206}Pb/^{204}Pb$ = 18.120–18.693, $^{207}Pb/^{204}Pb$ = 15.560–15.882 and $^{207}Pb/^{204}Pb$ = 38.207–39.586; Bao et al. [26]; Liu and Lin [36]; Zheng et al. [39,63]; Wang. [64]; Zhang et al. [65]; Fu [66]; Wang et al. [67]; Zhou et al. [68,69]) of typical carbonate hosted Zn-Pb deposits (e.g., Huize, Daliangzi, Tianbaoshan and Tianqiao deposit;) in S-Y-G Zn-Pb metallogenic province. In addition, In Pb-Pb diagrams (Figure 14a,b), the Pb isotopic data of the Nayongzhi deposit samples distribute in a narrow range, which is distinctly different from those Zn-Pb mineralization (e.g., Huize, Daliangzi, Tianbaoshan and Tianqiao deposit) associated with the Indosinian Orogeny in S-Y-G district. The Pb isotopic evidence indicates that it is impossible that the ore-forming metal of Nayongzhi deposit and other deposits in S-Y-G district are derived from an identical source.

Consequently, the geological features, Ag content of sphalerite and the Pb isotopic composition of sulfides (pyrite, galena and sphalerite) indicate that the Nayongzhi deposit is unlikely a product of the Indosinian Orogeny. Multistage Zn-Pb mineralization may occur in the S-Y-G district, which still need a precise geochronology to verify in the future.

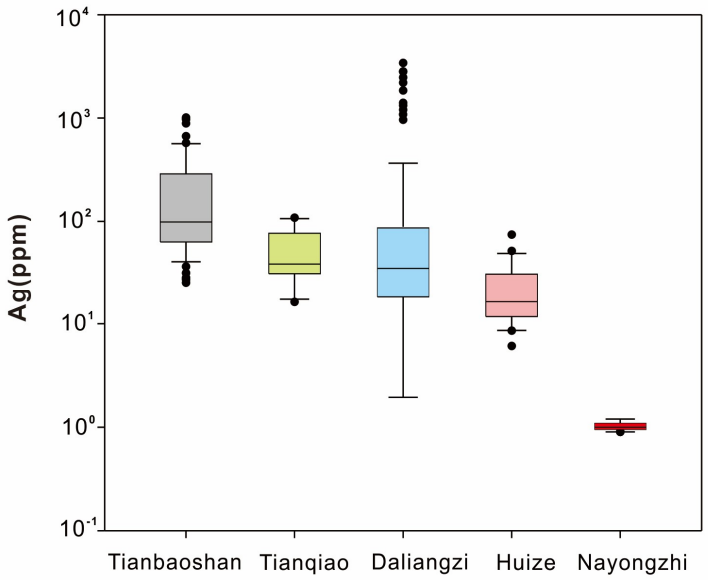

Figure 13. Ag content of sphalerite from Tianbaoshan, Daliangzi, Huize, Tianqiao and Nayongzhi deposit in S-Y-G Zn-Pb metallogenic province. Note: plots are based on data from Ye et al. [5,15], Li et al. [70] and Yuan et al. [71]. Minimum, maximum, median, lower quartile and upper quartile are indicated by the lowest point, the uppermost point, the line across the rectangular box, the upper boundary of the rectangular box, the lower boundary of the rectangular box of each column, respectively.

Table 3. Geological feature, ore-forming fluids and age of the typical MVT deposits in S-Y-G metallogenic province.

Deposit	Hosting Strata	Resources and Grade (Zn + Pb)	Metal Association	Morphology of Ore Bodies	Ore-Controlling Structure	Ore Texture	Mineral Assemblage	Ore-Forming Fluids	Timing of Mineralization (Ma)	Reference
Huize	Carboniferous dolostone	7 Mt, >25 wt %	Zn-Pb-Ag-Ge-Ga-Cd	veins and lenses	NE-trending thrust faults	Massive, disseminated	Ore minerals: sphalerite, galena and pyrite; gangue main minerals: dolomite, calcite and minor quartz	Th: 165–220 °C; salinity: 6.0–12.0 wt % NaCl eqv.	222; 220; 226	Zhou et al. [27]; Han et al. [28]; Li et al. [72]; Yin et al. [73]
Daliangzi	Sinian dolostone	4.5 Mt, 10–12 wt %	Zn-Pb-Ag-Ge-Ga-Cd	Vertical pipe-like	NW-trending wedging thrust faults	Massive, disseminated	Ore minerals: sphalerite, galena and pyrite; gangue main minerals: dolomite, calcite	Th: 170–225 °C; salinity: 18.0 wt % NaCl eqv.	204.4	Wu. [32]; Zheng et al. [39]; Zhang et al. [74]
Tianbaoshan	Sinian dolostone	2.6 Mt, 10–15 wt %	Zn-Pb-Ag-Ge-Ga-Cd	Vertical pipe-like	NNE-trending wedging thrust faults	Massive, disseminated, brecciated	Ore minerals: sphalerite, galena and pyrite, chalcopyrite; gangue main minerals: dolomite, calcite	Th: 157–167 °C; salinity: 12.4–20.0 wt % NaCl eqv.	early than 165 Ma	Wang et al. [67]; Zhang et al. [74]; Wang et al. [75]
Tianqiao	Devonian and Carboniferous dolostone	0.4 Mt, 15–18 wt %	Zn-Pb-Ag-Ge-Cd-Ag	Stratabound lenses	NW to NNW-trending thrust-fold faults	Massive, disseminated, banded	Ore minerals: sphalerite, galena and pyrite; gangue main minerals: dolomite, calcite	Th: 150–270 °C; salinity: 9.6–14.2 wt % NaCl eqv.	191.9	Zhou et al. [68,69,76]
Nayongzhi	Lower Cambrian dolostone	1.35 Mt, 4.6–7.5 wt %	Zn-Pb-Ga-Ge-Cd	Stratabound and bed-like	NE-trending anticline and faults	Disseminated, massive, brecciated	Ore minerals: sphalerite, galena and minor pyrite; gangue main minerals: dolomite, calcite and minor barite	Th: 100.5–165.4 °C; salinity: no data	No data	Jin et al. [17,24] and this study

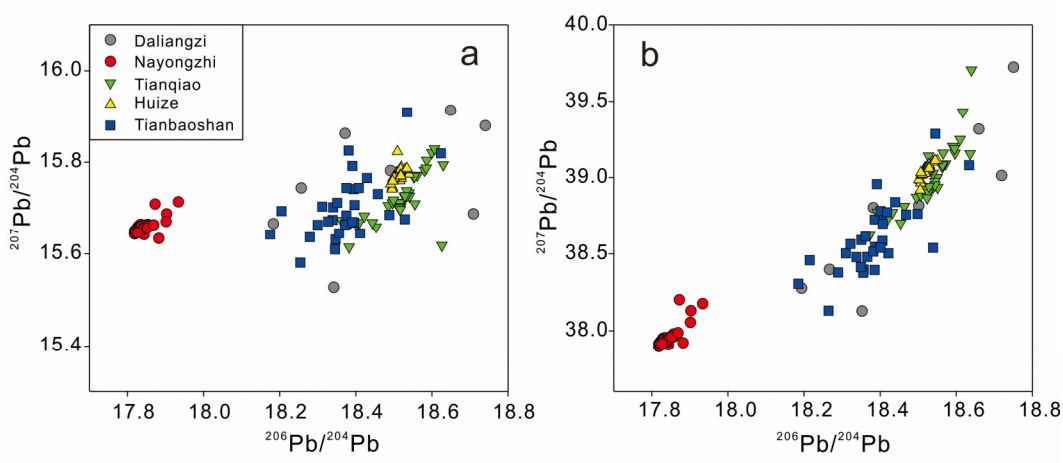

Figure 14. Correlative diagrams of $^{206}Pb/^{204}Pb$ VS. $^{207}Pb/^{204}Pb$ (**a**) and $^{206}Pb/^{204}Pb$ VS. $^{208}Pb/^{204}Pb$ (**b**) for the Tianbaoshan, Daliangzi, Huize, Tianqiao and Nayongzhi deposit in S-Y-G Zn-Pb metallogenic province. Note: plots are based on data from Jin et al. [17,24], Bao et al. [26], Liu and Lin [36], Zheng et al. [39,63], Chen et al. [62], Wang. [64], Zhang et al. [65], Fu [66], Wang et al. [67] and Zhou et al. [68,69].

7. Conclusions

To briefly summarize our main findings regarding the Nayongzhi deposit, we have shown the following:

1. Sphalerite from the Nayongzhi deposit is characterized by high contents of Cd, Ge and Ga, and low contents of Fe, Mn, In and Co. Those trace elements are present in the form of isomorphism in sphalerite; all datasets having been considered, notable coupled substitutions have been suggested from binary scatter plots and PCA: $Zn^{2+} \leftrightarrow Ga^{3+} + (Cu, Ag)^{+}$ and $Zn^{2+} \leftrightarrow In^{3+} + Sn^{3+} + \square$, although the Sn oxidation state still needs verification, and Fe is involved in direct $Zn^{2+} \leftrightarrow Fe^{2+}$ substitution.
2. The trace elements in sphalerite from this deposit are similar to those of the typical MVT deposit, with an ore-forming temperature range from 100.5 to 164.4 °C, which belongs to low-temperature mineralization.
3. Geological features, mineralogy and trace element contents in sphalerite indicate that the Nayongzhi deposit should be considered a MVT deposit.
4. Compared with geological characteristics, Ag content in sphalerite, and Pb isotopes, the Nayongzhi deposit is different from Zn-Pb deposits associated with the Indosinian Orogeny in S-Y-G district, suggesting multi-period Zn-Pb mineralization may have occurred in the region, although this is not verified by precise geochronology.

Author Contributions: C.W. and Z.H. proposed and organized the project. C.W., Z.H. and Z.Y. discussed and designed and performed the experiment. C.W. and Y.H. analyzed and interpreted the data. C.W. wrote the main manuscript. Z.H. and L.Y. revised the main manuscript. All the authors discussed the study.

Funding: This research was funded by the Sate Key Program of the Natural Science of China (Grant No.41430315) and the National "973" Program of China (2014CB440906).

Acknowledgments: The senior author is greatly indebted to the Derong Mining Ltd. for their permission to investigate and sample the Nayongzhi Zn-Pb Mine. We acknowledge three anonymous reviewers for their constructive reviews and valuable suggestions that led to great improvement in the presentation of the paper, and we extend our thanks to the editor of Minerals for their insightful comments.

Conflicts of Interest: The authors declare no conflict of interest.

Appendix A

Table A1. EMPA results of Sphalerite from the Nayongzhi deposit.

Sample No.	Zn (wt %)	S (wt %)	Fe (wt %)	Cd (wt %)	Ge (ppm)
SY-1290-9-1-1	65.32	32.85	0.33	0.20	700
SY-1290-9-1-1	64.54	32.54	0.86	0.22	n.d
SY-1290-9-1-2	64.21	32.9	1.27	0.18	n.d
SY-1290-9-1-3	65.59	32.56	0.72	0.21	n.d
SY-1290-9-2-2	64.23	33.79	0.55	0.23	n.d
SY-1290-9-2-3	64.50	33.21	0.44	0.2	n.d
SY-1290-9-2-4	64.53	32.68	0.76	0.18	n.d
SY-1290-9-2-5	64.93	32.59	0.83	0.25	n.d
SY-1290-9-2-6	64.93	32.7	0.45	0.36	n.d
SY-1270-9-2-7	65.57	32.95	0.92	0.2	n.d
SY-1270-9-2-8	65.35	33.14	0.6	0.24	n.d
SY-1290-9-2-9	64.76	32.88	1.19	0.22	n.d
SY-1270-10-1-1	64.04	32.52	1.29	0.18	n.d
SY-1270-10-1-2	64.79	32.45	0.94	0.19	n.d
SY-1270-10-1-3	65.63	31.98	2.28	n.d	n.d
SY-1290-9-3-1	64.21	32.9	1.27	n.d	n.d
SY-1290-9-3-2	63.85	33.04	1.88	0.12	n.d
SY-1290-9-3-3	64.63	32.98	2.28	n.d	n.d
SY-1290-9-3-4	63.85	33.04	1.88	n.d	n.d
SY-1290-9-3-5	64.97	32.61	1.08	n.d	n.d
SY-1290-9-3-6	64.76	32.88	1.19	n.d	n.d
SY-1290-9-3-7	63.85	33.04	1.88	n.d	n.d
SY-1290-9-3-8	64.95	33.61	1.28	n.d	n.d
LML-1270-10-1	63.85	33.04	1.88	n.d	500
LML-1270-10-2	64.76	32.88	1.19	n.d	n.d
LML-1270-10-3	65.63	31.98	2.28	n.d	n.d
LML-1270-10-4	64.04	33.52	1.29	n.d	n.d
LML-1270-10-5	63.61	33.66	1.9	n.d	n.d
LML-1270-10-6	64.90	32.98	2.07	0.11	n.d
LML-1270-10-7	64.04	33.52	1.29	n.d	n.d
LML-1270-10-8	64.04	33.52	1.29	0.14	n.d
LML-1270-10-9	63.90	33.33	1.94	n.d	n.d

Notes: n.d in the data table indicates that the content of the element is below the detection limit.

References

1. Moskalyk, R.R. Gallium: The backbone of the electronics industry. *Miner. Eng.* **2003**, *16*, 921–929. [CrossRef]
2. Alfantazi, A.M.; Moskalyk, R.R. Processing of indium: A review. *Miner. Eng.* **2003**, *16*, 687–694. [CrossRef]
3. Höll, R.; Kling, M.; Schroll, E. Metallogenesis of germanium—A review. *Ore Geol. Rev.* **2007**, *30*, 145–180. [CrossRef]
4. Cook, N.J.; Ciobanu, C.L.; Pring, A.; Skinner, W.; Shimizu, M.; Danyushevsky, L.; SainiEidukat, B.; Melcher, F. Trace and minor elements in sphalerite: A LA-ICPMS study. *Geochim. Cosmochim. Acta* **2009**, *73*, 4761–4791. [CrossRef]
5. Ye, L.; Cook, N.J.; Ciobanu, C.L.; Liu, Y.P.; Zhang, Q.; Liu, T.G.; Gao, W.; Yang, Y.L.; Danyushevsky, L. Trace and minor elements in sphalerite from base metal deposits in South China: A LA-ICPMS study. *Ore Geol. Rev.* **2011**, *39*, 188–217. [CrossRef]
6. Belissont, R.; Boiron, M.C.; Luais, B.; Cathelineau, M. LA-ICP-MS analyses of minor and trace elements and bulk Ge isotopes in zoned Ge-rich sphalerites from the Noailhac-Saint-Salvy deposit (France): Insights into incorporation mechanisms and ore deposition processes. *Geochim. Cosmochim. Acta* **2014**, *126*, 518–540. [CrossRef]
7. Frenzel, M.; Hirsch, T.; Gutzmer, J. Gallium, germanium, indium, and other trace and minor elements in sphalerite as a function of deposit type—A meta-analysis. *Ore Geol. Rev.* **2016**, *76*, 52–78. [CrossRef]

8. Mondillo, N.; Arfè, G.; Herrington, R.; Boni, M.; Wilkinson, C.; Mormone, A. Germanium enrichment in supergene settings: Evidence from the Cristal nonsulfide Zn prospect, Bongará district, northern Peru. *Miner. Depos.* **2018**, *53*, 155–169. [CrossRef]
9. Mohund, G.H.; Jager, A. Phasengleichgewichte des systems Ge-Pb-Zn-S in relation zu germanium-gehalten alpiner Pb-Zn-Lagerstatten. *Verh. Geol. Bundesanst.* **1978**, *34*, 437–440.
10. Cook, N.J.; Ciobanu, C.L.; Brugger, J.; Etschmann, B.; Howard, D.L.; De Jonge, M.D.; Ryan, C.; Paterson, D. Determination of the oxidation state of Cu in substituted Cu In-Fe-bearing sphalerite via μ-XANES spectroscopy. *Am. Miner.* **2012**, *97*, 476–479. [CrossRef]
11. Belissont, R.; Muñoz, M.; Boiron, M.C.; Luais, B.; Mathon, O. Distribution and oxidation state of Ge, Cu and Fe in sphalerite by μ-XRF and K-edge μ-XANES: Insights into Ge incorporation, partitioning and isotopic fractionation. *Geochim. Cosmochim. Acta* **2016**, *177*, 298–314. [CrossRef]
12. Oftedal, I. Untersuchungen über die Nebenbestandteile von Erzmineralen norwegischer zinkblende-führender Vorkommen. Skrifter utgit av Det Norske Videnskaps-Akademi i Oslo, I. Mat. *Nat. Kl.* **1941**, *8*, 103.
13. Warren, H.V.; Thompson, R.M. Sphalerites from western Canada. *Econ. Geol.* **1945**, *40*, 309–335. [CrossRef]
14. Möller, P. Correlation of homogenization temperatures of accessory minerals from sphalerite-bearing deposits and Ga/Ge model temperatures. *Chem. Geol.* **1987**, *61*, 153–159. [CrossRef]
15. Ye, L.; Li, Z.L.; Hu, Y.S.; Huang, Z.L.; Zhou, Z.J.; Fan, H.F.; Danyushevskiy, L. Trace element in sulfide from Tianbaoshan Pb-Zn deposit, Sichuan province, China: A LA-ICPMS study. *Acta Petrol. Sin.* **2016**, *32*, 3377–3393. (In Chinese)
16. Zhang, Q. Trace elements in galena and sphalerite and their geochemical significance in distinguishing the genetic types of Pb–Zn ore deposits. *Chin. J. Geochem.* **1987**, *6*, 177–190.
17. Jin, Z.G.; Zhou, J.X.; Huang, Z.L.; Luo, K.; Gao, J.G.; Peng, S.; Wang, B.; Chen, X.L. Ore gensis of the Nayongzhi deposit, Puding City, Guizhou Province, China: Evidences from S and in situ Pb istopes. *Acta Petrol. Sin.* **2016**, *32*, 3441–3455. (In Chinese)
18. Zhou, J.X.; Wang, X.C.; Wilde, S.A.; Luo, K.; Huang, Z.L.; Wu, T.; Jin, Z.G. New insights into the metallogeny of MVT Zn-Pb deposits: A case study from the Nayongzhi in South China, using field data, fluid compositions, and in situ S-Pb isotopes. *Am. Miner.* **2018**, *103*, 91–108. [CrossRef]
19. Tan, H. Geological Characteristics and Analysis on Prospecting for Lead-Zinc Deposits, Wuzhishan area, Guizhou. *Guizhou Geol.* **2007**, *24*, 253–257. (In Chinese)
20. Zou, J.B.; Xiao, L.; Gui, Z. Geologic characters and control factors of lead-zinc deposit in Wuzhishan, Guizhou. *Guizhou Geol.* **2009**, *26*, 101–105. (In Chinese)
21. Huang, L.; Zhang, K. Analysis on the ore control factors, metallogenic regulation and prospecting direction of Shuidong-wuzhishan Lead-zinc deposit of northwest Guizhou. *Guizhou Geol.* **2010**, *27*, 203–207. (In Chinese)
22. Wu, X.B.; Zhu, Y.Q.; Liao, S.H.; Shuo, R.Q. Geological characteristics and prospecting potential of Nayongzhi Pb-Zn deposit in Wuzhishan anticline. *Miner. Resour. Geol.* **2013**, *27*, 26–31. (In Chinese)
23. Chen, G.Y.; Wang, L.; Fan, Y.M.; Zheng, W. Ore-search prospect of the deep subsurface in the Wuzhishan Pb-Zn orefield, Guizhou province. *J. Geochem. Explor.* **2015**, *51*, 858–869. (In Chinese)
24. Jin, C.H.; Li, K.; Huang, L.; Zhang, Y.; Shen, Z.W. Characteristics of sulfur and lead isotopic composition and metallogenic material source of the Nayongzhi Pb-Zn deposit, northwestern Guizhou Province. *J. Miner. Petrol.* **2015**, *35*, 81–88. (In Chinese)
25. Peng, S.; Jin, Z.G.; Lin, G.S.; Zhu, Y.Q.; Wang, B. Analysis of ore-controlling factors and metallogenic model of Wuzhishan lead-zinc deposit, Guizhou: Case study of Nayongzhi deposit. *Miner. Explor.* **2016**, *7*, 463–470. (In Chinese)
26. Bao, Z.; Li, Q.; Wang, C.Y. Metal source of giant Huize Zn-Pb deposit in SW China: New constraints from in situ Pb isotopic compositions of galena. *Ore Geol. Rev.* **2017**. [CrossRef]
27. Zhou, C.X.; Wei, C.S.; Guo, J.Y. The source of metals in the Qilingchang Pb-Zn deposit, Northeastern Yunnan, China: Pb-Sr isotope constraints. *Econ. Geol.* **2001**, *96*, 583–598. [CrossRef]
28. Han, R.S.; Liu, C.Q.; Huang, Z.L.; Chen, J.; Ma, D.Y.; Lei, L.; Ma, G.S. Geological features and origin of the Huize carbonate-hosted Zn-Pb-(Ag) District, Yunnan, South China. *Ore Geol. Rev.* **2007**, *31*, 360–383. [CrossRef]

29. Sun, W.H.; Zhou, M.F.; Gao, G.F.; Yang, Y.H.; Zhao, X.F.; Zhao, J.H. Detrital zircon U-Pb geochronological and Lu-Hf isotopic constraints on the Precambrian magmatic and crustal evolution of the western Yangtze Block, SW China. *Precambrian Res.* **2009**, *172*, 99–126. [CrossRef]
30. Zhao, X.F.; Zhou, M.F.; Li, J.W.; Sun, M.; Gao, J.F.; Sun, W.H.; Yang, J.H. Late Paleoproterozoic to early Mesoproterozoic Dongchuan Group in Yunnan, SW China: Implications for tectonic evolution of the Yangtze Block. *Precambrian Res.* **2010**, *182*, 57–69. [CrossRef]
31. Yan, D.P.; Zhou, M.F.; Song, H.L.; Wang, X.W.; Malpas, J. Origin and tectonic significance of a Mesozoic multi-layer over-thrust system within the Yangtze Block (South China). *Tectonophysics* **2003**, *361*, 239–254. [CrossRef]
32. Wu, Y. The Age and Ore-Forming Process of MVT Deposits in the Boundary Area of Sichuan-Yunnan-Guizhou Provinces, Southwest China. Ph.D. Thesis, China University of Geosciences, Beijing, China, 2013; pp. 1–167. (In Chinese)
33. He, B.; Xu, Y.G.; Huang, X.L.; Luo, Z.Y.; Shi, Y.R.; Yang, Q.J.; Yu, S.Y. Age and duration of the Emeishan flood volcanism, SW China: Geochemistry and SHRIMP zircon U-Pb dating of silicic ignimbrites, post-volcanic Xuanwei Formation and clay tuff at the Chaotian section. *Earth Planet. Sci. Lett.* **2007**, *255*, 306–323. [CrossRef]
34. Chung, S.L.; Jahn, B.M. Plume-lithosphere interaction in generation of the Emeishan flood basalts at the Permian-Triassic boundary. *Geology* **1995**, *23*, 889–892. [CrossRef]
35. Zhou, M.F.; Yan, D.P.; Kennedy, A.K.; Li, Y.Q.; Ding, J. SHRIMP zircon geochronological and geochemical evidence for Neo-proterozoic arc-related magmatism along the western margin of the Yangtze Block, South China. *Earth Planet. Sci. Lett.* **2002**, *196*, 51–67. [CrossRef]
36. Liu, H.C.; Lin, W.D. *Study on the Law of Pb-Zn-Ag Ore Deposit in Northeast Yunnan*; Yunnan University Press: Kunming, China, 1999; pp. 1–468. (In Chinese)
37. Han, R.S.; Zou, H.J.; Hu, B.; Hu, Y.Z.; Xue, C.D. Features of fluid inclusions and sources of ore-forming fluid in the Maoping carbonate-hosted Zn-Pb-(Ag-Ge) deposit, Yunnan, China. *Acta Petrol. Sin.* **2007**, *23*, 2109–2118. (In Chinese)
38. Han, R.S.; Hu, Y.Z.; Wang, X.K.; Hou, B.H.; Huang, Z.L.; Chen, J.; Wang, F.; Wu, P.; Li, B.; Wang, H.J.; Dong, Y.; et al. Mineralization model of rich Ge-Ag bearing Zn-Pb polymetallic deposit concentrated district in northeastern Yunnan, China. *Acta Geol. Sin.* **2012**, *86*, 280–294. (In Chinese)
39. Zheng, M.H.; Wang, X.C. Genesis of the Daliangzi Pb-Zn deposit in Sichuan, China. *Econ. Geol.* **1991**, *86*, 831–846. [CrossRef]
40. Qi, L.; Hu, J.; Gregoire, D.C. Determination of trace elements in granites by inductively coupled plasma mass spectrometry. *Talanta* **2000**, *51*, 507–513.
41. Le Maitre, R.W. *Numerical Petrology: Statistical Interpretation of Geochemical Data*; Elsevier: Amsterdam, The Netherlands, 1982.
42. Koch, I. *Analysis of Multivariate and High-Dimensional Data Theory and Practice*; Cambridge University Press: Cambridge, UK, 2012.
43. Samama, J.C.; Royer, J.J.; N'Ganzi, C. Prise en compte de la surface specifique des pre levements en prospection geochimique: Exemple de luranium dans les sediments deruisseau. *J. Geochem. Explor.* **1989**, *32*, 453–466. [CrossRef]
44. Cadoux, A.; Blichert-Toft, J.; Pinti, D.L.; Albarede, F. A unique lower mantle source for Southern Italy volcanics. *Earth Planet. Sci. Lett.* **2007**, *259*, 227–238. [CrossRef]
45. Iwamori, H.; Albarede, F.; Nakamura, H. Global structure of mantle isotopic heterogeneity and its implications for mantle differentiation and convection. *Earth Planet. Sci. Lett.* **2010**, *299*, 339–351. [CrossRef]
46. Winderbaum, L.; Ciobanu, C.L.; Cook, N.J.; Paul, M.; Metcalfe, A.; Gilbert, S. Multivariate analysis of an LA-ICP-MS trace element dataset for pyrite. *Math. Geosci.* **2012**, *44*, 823–842. [CrossRef]
47. Cook, N.J.; Sundblad, K.; Valkama, M.; Nygård, R.; Ciobanu, C.L.; Danyushevsky, L. Indium mineralization in A-type granites in southeastern Finland: Insights into mineralogy and partitioning between coexisting minerals. *Chem. Geol.* **2011**, *284*, 62–73. [CrossRef]
48. George, L.L.; Cook, N.J.; Ciobanu, C.L. Partitioning of trace elements in co-crystallized sphalerite-galena-chalcopyrite hydrothermal ores. *Ore Geol. Rev.* **2016**, *77*, 97–116. [CrossRef]
49. Epple, M.; Panthofer, M.; Walther, R.; Deiseroth, H.J. Crystal-chemical characterization of mixed valence indium chalcogenides by X-ray absorption spectroscopy (EXAFS). *Int. J. Struct. Phys. Chem. Asp. Cryst. Mater.* **2000**, *215*, 445–453.

50. Goh, S.W.; Buckley, A.N.; Lamb, R.N. Copper (II) sulphide? *Miner. Eng.* **2006**, *19*, 204–208. [CrossRef]
51. Di Benedetto, F.; Andreozzi, G.B.; Bernadini, G.P.; Borgheresi, M.; Caneschi, A.; Cipciani, C.; Gatteschi, D.; Romanelli, M. Short range order of Fe^{2+} impurities, isolated and in pairs, in ZnS and CdS studies by the Mossbauer effect. Phys. *Chem. Miner.* **2005**, *32*, 339–348.
52. Wright, K.V.; Gale, J.D. A first principles study of the distribution of iron in sphalerite. *Geochim. Cosmochim. Acta* **2010**, *74*, 3514–3520. [CrossRef]
53. Bernstein, L.R. Germanium geochemistry and mineralogy. *Geochim. Cosmochim. Acta* **1985**, *49*, 2409–2422. [CrossRef]
54. Johan, Z. Indium and germanium in the structure of sphalerite: An example of coupled substitution with copper. *Miner. Petrol.* **1988**, *39*, 211–229. [CrossRef]
55. Ye, L.; Cook, N.J.; Liu, T.G.; Ciobanu, C.L.; Gao, W.; Yang, Y. The Niujiaotang Cd-rich zinc deposit, Duyun, Guizhou province, Southwest China: Ore genesis and mechanisms of cadmium concentration. *Miner. Depos.* **2012**, *47*, 1–18. [CrossRef]
56. Wei, C. Ore-forming Fluid and Ore Genesis of the Nayongzhi Deposit in Northwestern Guizhou, China. Master's Thesis, University of Chinese Academy of Sciences and for the Diploma of Institute of Geochemistry, Guiyang, China, 2018; pp. 1–114. (In Chinese)
57. Leach, D.L.; Sangster, D.F.; Kelley, K.D.; Large, R.R.; Garven, G.; Allen, C.R.; Gutzmer, J.; Walters, S. Sediment-hosted lead-zinc deposits: A global perspective. *Econ. Geol.* **2005**, *100*, 561–607.
58. Leach, D.L.; Sangster, D.F. Mississippi Valley-type lead-zinc deposits. In *Mineral Deposit Modeling*; Kirkhan, R.V., Sinclair, W.D., Thorpe, R.I., Duke, J.M., Eds.; Special Paper; Geological Association of Canada: St. John's, NL, Canada, 1993.
59. Leach, D.L.; Bradley, D.; Lewchuk, M.T.; Symons, D.T.; de Marsily, G.; Brannon, J. Mississippi Valley-type lead-zinc deposits through geological time: Implications from recent age-dating research. *Miner. Depos.* **2001**, *36*, 711–740. [CrossRef]
60. Zhang, C.Q.; Wu, Y.; Hou, L.; Mao, J.W. Geodynamic setting of mineralization of Mississippi Valley-type deposits in world-class Sichuan-Yunnan-Guizhou Zn-Pb triangle, southwest China: Implications from age-dating studies in the past decade and the Sm-Nd age of Jinshachang deposit. *J. Asian Earth Sci.* **2015**, *103*, 103–114.
61. Hu, R.Z.; Fu, S.L.; Huang, Y.; Zhou, M.F.; Fu, S.H.; Zhao, C.H.; Wang, Y.J.; Bi, X.W.; Xiao, J.F. The giant South China Mesozoic low-temperature metallogenic domain: Reviews and a new geodynamic model. *J. Asian Earth Sci.* **2016**, *137*, 9–34. [CrossRef]
62. Chen, W.; Kong, Z.G.; Liu, F.X.; Wang, X.W.; Deng, M.G.; Zhao, J.X.; Liu, Y.; Zhang, X.H. Geology, Geochemistry ore and Genesis of the Nayongzhi Pb-Zn deposit, Guizhou Province, NW China. *Acta Geol. Sin.* **2017**, *91*, 1269–1284. (In Chinese)
63. Zheng, C.L. An approach on the source of ore-forming metals of lead-zinc deposits in Northwestern part, Guizhou, Province. *J. Guilin Coll. Geol.* **1994**, *14*, 113–124. (In Chinese)
64. Wang, H.Y. Geochemistry of Pb–Zn mineralization in Guizhou. *Guizhou Geol.* **1993**, *10*, 272–290. (In Chinese)
65. Zhang, Q.H.; Mao, J.Q.; Guang, S.Y. The studies of ore-forming material sources of metal deposit in Hezhang Pb-Zn mine Shuicheng, Guizhou province. *J. Guizhou Univ. Technol.* **1998**, *27*, 26–34. (In Chinese)
66. Fu, S.H. Metallogenesis of Pb-Zn Deposits and Enrichment Regularity of Dispersed Elements Cd, Ga and Ge in SW Yangtze Block. Ph.D. Thesis, Chengdu University of Science and Technology, Chengdu, China, 2004; pp. 20–67. (In Chinese)
67. Wang, X.C.; Zheng, Z.R.; Zheng, M.H.; Xu, X.H. Metallogenic mechanism of the Tianbaoshan Pb-Zn deposit, Sichuan. *Chin. J. Geochem.* **2000**, *19*, 121–133. [CrossRef]
68. Zhou, J.X.; Huang, Z.L.; Zhou, M.F.; Li, X.B.; Jin, Z.G. Constraints of C-O-S-Pb isotope compositions and Rb-Sr isotopic age on the origin of the Tianqiao carbonate-hosted Pb-Zn deposit, SW China. *Ore Geol. Rev.* **2013**, *53*, 77–92. [CrossRef]
69. Zhou, J.X.; Gao, J.G.; Chen, Da.; Liu, X.K. Ore genesis of the Tianbaoshan carbonate-hosted Pb-Zn deposit, Southwest China: Geologic and isotopic (C-H-O-S-Pb) evidence. *Int. Geol. Rev.* **2013**, *55*, 1300–1310. [CrossRef]
70. Li, Z.L.; Ye, L.; Huang, Z.L.; Nian, H.L.; Zhou, J.X. Primary research on trace elements in sphalerite from Tianqiao Pb-Zn deposit, northwestern Guizhou province, China. *Acta Geosci. Sin.* **2016**, *36*, 183–186. (In Chinese)

71. Yuan, B.; Zhang, C.Q.; Yu, H.J.; Yang, Y.M.; Zhao, Y.X.; Zhu, C.C.; Ding, Q.F.; Zhou, Y.B.; Yang, J.C.; Xu, Y. Element enrichment characteristics: Insights from element geochemistry of sphalerite in Daliangzi Pb-Zn deposit, Sichuan, Southwest China. *J. Geochem. Explor.* **2017**, *186*, 187–201. [CrossRef]
72. Li, W.B.; Huang, Z.L.; Wang, Y.X.; Chen, J.; Han, R.S.; Xu, C.; Guan, T.; Yin, M.D. Age of the giant Huize Pb-Zn deposits determined by Sm-Nd dating of hydrothermal calcite. *Geol. Rev.* **2004**, *50*, 189–195. (In Chinese)
73. Yin, M.D.; Li, W.B.; Sun, X.W. Rb-Sr isotopic dating of sphalerite from the giant Huize Zn–Pb ore field, Yunnan Province, Southwestern China. *Chin. J. Geochem.* **2009**, *28*, 70–75. [CrossRef]
74. Zhang, C.Q. The Genetic Model of Mississippi Valley-Type Deposits in the Boundary Area of Sichuan, Yunnan and Guizhou Province, China. Ph.D. Thesis, Chinese Academy of Geological Sciences, Beijing, China, 2008; pp. 1–177. (In Chinese)
75. Wang, R.; Zhang, C.Q.; Wu, Y. A discussion on relationship between the age of Diabase dyke and Pb-Zn mineralization in Tanbaoshan Pb-Zn deposit, Sichuan. *Miner. Depos.* **2012**, *31*, 449–450. (In Chinese)
76. Zhou, J.X. Geochemistry of Dispersed Elements and Zinc Isotope in Carbonate-hosted Lead-Zinc Ore Deposits District, Northwest Guizhou Province, China. Ph.D. Thesis, Chinese Academy of Sciences and for the Diploma of Institute of Geochemistry, Guiyang, China, 2011; pp. 1–124. (In Chinese)